Human iPSC modeling reveals mutation-specific responses to gene therapy in Best disease

Divya Sinha[a,b,1], Benjamin Steyer[a,c,1], Pawan K. Shahi[a,d], Katherine Mueller[c], Rasa Valiauga[b], Kimberly L. Edwards[b], Cole Bacig[b], Stephanie S. Steltzer[c], Sandhya Srinivasan[c], Amr Abdeen[c], Evan Cory[c], Viswesh Periyasamy[c], Alireza Fotuhi Siahpirani[c], Edwin M. Stone[e], Budd A Tucker[e], Sushmita Roy[c,f], Bikash R. Pattnaik[a,d,g,2], Krishanu Saha[a,c,h,2], David M. Gamm[a,b,g,2,3]

[a]McPherson Eye Research Institute, University of Wisconsin-Madison, Madison, WI, USA 53705

[b]Waisman Center, University of Wisconsin-Madison, Madison, WI, USA 53705

[c]Wisconsin Institute for Discovery, University of Wisconsin-Madison, Madison, WI, USA 53715

[d]Department of Pediatrics, University of Wisconsin-Madison, Madison, WI, USA 53792

[e]Department of Ophthalmology and Visual Sciences, Carver College of Medicine, Iowa City, IA 52242

[f]Department of Biostatistics, University of Wisconsin-Madison, Madison, WI, USA 53792

[g]Department of Ophthalmology and Visual Sciences, University of Wisconsin-Madison, Madison, WI, USA 53705

[h]Department of Biomedical Engineering, University of Wisconsin-Madison, Madison, WI, USA 53706

[1]These authors contributed equally to the work

[2]**Co-Correspondence:**

David M. Gamm

1500 Highland Avenue, Madison, WI, USA 53705

E-mail: dgamm@wisc.edu; Phone: 608-261-1516

Krishanu Saha

330 N. Orchard Street,

Madison WI, USA 53715

E-mail: ksaha@wisc.edu; Phone: 608-316-4313

Bikash R. Pattnaik

1300 University Avenue, Madison, WI, USA 53706

E-mail: pattnaik@wisc.edu; Phone: 608-265-9486

[3]**Lead contact:** David M. Gamm

Keywords: human pluripotent stem cells, gene therapy, gene augmentation, autosomal dominant disease, macular degeneration, orphan disease, channelopathy, somatic cell gene editing, CRISPR-Cas9

Abstract: Dominantly inherited disorders are not typically considered therapeutic candidates for gene augmentation. Here, we utilized patient-specific induced pluripotent stem cell-derived retinal pigment epithelium (iPSC-RPE) to test the potential of gene augmentation to treat Best disease, a dominant macular dystrophy caused by over 200 missense mutations in *BEST1*. Gene augmentation in iPSC-RPE fully restored BEST1 calcium-activated chloride channel activity and improved rhodopsin degradation in iPSC-RPE models of recessive bestrophinopathy and dominant Best disease caused by two different ion binding domain mutations. A dominant Best disease iPSC-RPE model that did not respond to gene augmentation showed normalization of BEST1 channel activity following CRISPR-Cas9 editing of the mutant allele. We then tested gene editing in all three dominant Best disease iPSC-RPE models, which produced premature stop codons exclusively within the mutant *BEST1* alleles. Single-cell profiling demonstrated no adverse perturbation of RPE transcriptional programs in any model, although off-target analysis detected a silent genomic alteration in one model. These results suggest that gene augmentation is a viable first-line approach for some dominant Best disease patients and that non-responders are candidates for alternate approaches such as genome editing. However, testing genome editing strategies

for on-target efficiency and off-target events using patient-matched iPSC-RPE model systems is warranted. In summary, personalized iPSC-RPE models can be used to select among a growing list of gene therapy options to maximize safety and efficacy while minimizing time and cost. Similar scenarios likely exist for other genotypically diverse channelopathies, expanding the therapeutic landscape for affected patients.

Introduction: Genotypically heterogeneous dominant diseases pose significant challenges and opportunities for precision medicine (1). Among gene therapies, gene augmentation for recessive disorders is the most developed, having spurred multiple clinical trials (2-4) and FDA approval for one ocular disease (5). However, gene augmentation is generally ruled out as a stand-alone therapy for dominant disorders due to a perceived need to eliminate the deleterious effects of the mutant allele. Gene editing approaches to silence or repair mutant alleles hold promise in this regard (6-8), but testing safety and efficacy for every mutant allele-specific genome editor presents practical and economic challenges in diseases with high mutational diversity. Further, gene editing may not be able to target all mutations (6, 9, 10) and could lead to off-target mutagenesis—particularly within a heterozygous wildtype allele—or other adverse events (11). Another consideration for gene therapy development is the need for preclinical model systems with phenotypes and/or genotypes that are relevant to the human disease. This requirement is particularly challenging for genome editing strategies, which utilize sequence-specific tools and thus require human model systems to test safety and efficacy (12). Humanized animal models have also been employed for this purpose (13), although they cannot be used for genome-wide off-target analysis.

One disorder that faces a full array of these therapeutic obstacles is Best disease, a major cause of inherited macular degeneration that currently has no treatment options. Best disease exclusively targets the retinal pigment epithelium (RPE), a monolayer of cells essential for the survival and function of

70 photoreceptors. Although Best disease is often diagnosed in early childhood based on its distinctive
71 ophthalmological findings (14), its effects on central vision are generally mild at first. Vision loss occurs
72 progressively and irreversibly over several decades, thus providing a wide time window for therapeutic
73 intervention.

74 Best disease is a genotypically diverse disorder transmitted primarily in an autosomal dominant
75 fashion, although rare cases of autosomal recessive bestrophinopathy (ARB) are known (15). Together,
76 autosomal dominant Best disease (adBD) and ARB are linked to over 200 mutations in the *BEST1* gene,
77 which encodes a putative homo-pentameric calcium-activated chloride channel (CaCC) found in the RPE.
78 Recent elucidation of the high-resolution crystal structure of chicken Best1 reinforced its role as a CaCC
79 and revealed that disease-associated mutations cluster within calcium or chloride ion binding sites or
80 within structural regions of the channel (16).

81 A significant impediment to the development of therapies for adBD is the lack of model systems
82 that adequately mimic the genotypic and phenotypic characteristics of the disorder. While canine models
83 of ARB mirror the human ARB phenotype (14), no suitable animal models of adBD exist. To provide a
84 therapeutic testing platform for adBD, we previously developed the first human iPSC-RPE models of the
85 disease, which demonstrated relevant cellular dysfunction; most notably, delayed degradation of
86 phagocytosed photoreceptor outer segment (POS) proteins (17, 18). These adBD iPSC-RPE models were
87 then used to test the potential for selected pharmacological interventions to ameliorate the cellular
88 phenotype of this disorder (18).

89 In the present study, we examined whether gene therapy could definitively correct the functional
90 defects present in adBD iPSC-RPE. Given that BEST1 forms a homo-pentameric CaCC, we hypothesized
91 that gene augmentation could potentially mitigate the cellular disease phenotype in adBD by increasing
92 the ratio of wild-type to mutant BEST1 monomers available for channel assembly. This theory presumes

that the deleterious effects of the mutant allele can be diluted sufficiently to restore CaCC function, preferably in a controlled manner without the risks associated with unregulated transgene expression.

To test our hypothesis, we employed three iPSC-RPE models of adBD, along with one iPSC-RPE model of ARB as a control. Importantly, the iPSC lines were generated from patients with *BEST1* mutations in different functional regions of the channel (*i.e.*, calcium binding, chloride binding, and structural) (16). We then ectopically expressed wildtype *BEST1* in iPSC-RPE using a viral vector that incorporated the native *BEST1* promoter, *VMD2*, in order to maintain RPE specificity and to keep transgene expression levels in check. Using this strategy, we obtained a >3-fold increase in wildtype BEST1 protein expression across all adBD iPSC-RPE models. Single cell electrophysiology and cell population-based assays revealed that two of the adBD mutations were exceedingly responsive to gene augmentation alone. Indeed, the correction of the cellular disease phenotype observed in these adBD iPSC-RPE models following gene augmentation was on par with that seen in the ARB iPSC-RPE model.

To address the adBD mutation that failed to respond to gene augmentation, as well as others that may also be refractory to this broad therapeutic strategy, we examined whether CRISPR-Cas9 gene editing could specifically target the mutant *BEST1* allele, leaving the normal allele intact. We found that gene editing was highly efficient at eliminating mutant allele expression and restoring iPSC-RPE CaCC activity in all three adBD models. These results bode well for the use of CRISPR-Cas9 to treat adBD mutations that are not candidates for gene augmentation, contingent on the availability of suitable guide RNAs. We then investigated whether gene editing caused untoward effects on the RPE transcriptome or induced off-target genome alterations in any of the adBD models. While no transcriptomic perturbations were detected, a single significant—albeit functionally silent—off-target site contained genomic insertions and deletion mutations (indels) in one adBD model. Based on our findings, we propose a two-tiered approach to adBD gene therapy that uses iPSC-RPE testing to first determine which mutations are

likely to respond to frontline treatment with gene augmentation. *BEST1* mutant iPSC-RPE models that do not demonstrate phenotypic correction with gene augmentation would then undergo next-level safety and efficacy testing to assess candidacy for customized genome editing.

Results

BEST1 mutations decrease CaCC activity in patient-specific iPSC-RPE.

In addition to the N926H and A146K adBD iPSC lines previously reported (17, 18), we generated iPSCs from a third adBD patient with an R218C mutation and an ARB patient with compound heterozygous mutations (R141H/A195V) (**Figure 1A**). Based on the crystallographic studies, each of these mutations lies within a different functional region of the BEST1 channel (**Figure 1B**) (16). We also employed two control iPSC lines: a wildtype (WT) iPSC line and an isogenic iPSC line generated via CRISPR-based gene correction of R218C adBD iPSCs (R218C>WT) (19). All six iPSC lines were tested for pluripotency, differentiated to RPE, and characterized (**Figures 1C-D, and S1A-D**). iPSC-RPE monolayers for all adBD and control lines, but not the ARB line, showed robust levels of BEST1 protein expression (**Figure 1D**). The profoundly decreased BEST1 level in our ARB cultures is consistent with reports using heterologous expression or iPSC-RPE systems that showed low or undetectable levels of R141H or A195V BEST1 (20, 21). As a measurement of CaCC activity, single-cell patch-clamp recordings of calcium-activated chloride current density were performed and found to be greatly diminished in all patient-specific iPSC-RPE relative to WT control iPSC-RPE (**Figures 1E and S1E-I**). Gene-corrected R218C>WT isogenic iPSC-RPE control showed CaCC current density at levels similar to native WT control lines (**Figures 1E and S1J**), indicating that the decreased CaCC activity was indeed the result of the BEST1 mutation.

139 ***BEST1* augmentation restores CaCC activity and enhances rhodopsin degradation in ARB iPSC-**
140 **RPE.**

141 We next sought to confirm that ectopic expression of WT human BEST1 (hBEST1) could
142 ameliorate the disease phenotype of R141H/A195V ARB iPSC-RPE, analogous to gene augmentation
143 studies using ARB canines or other iPSC-RPE model systems for ARB (22, 23). Single-cell patch clamp
144 recordings of calcium-activated chloride current density were used as a readout of efficacy in iPSC-RPE
145 cells. In addition, we monitored degradation of rhodopsin following POS feeding as an assay of intact
146 RPE monolayer function.

147 For gene augmentation we used a lentivirus construct (*hVMD2-hBEST1-T2A-GFP*) designed to
148 co-express hBEST1 and green fluorescent protein (GFP) under control of the human *BEST1* promoter
149 (*hVMD2*), which assures both RPE-specific expression and *BEST1*-specific gene regulation (**Figures 2A,**
150 **B**). Lentivirus was chosen for transgene delivery based on its safe use in human retinal gene therapy trials
151 (24) (ClinicalTrials.gov Identifiers: NCT01367444, NCT01736592) and its superior transduction
152 efficiency in cultured human RPE (17, 25). GFP expression was observed in ARB iPSC-RPE cells post-
153 transduction, and immunocytochemical (ICC) and western blot analysis confirmed enhanced expression
154 of BEST1 in treated cultures (**Figures 2C, S2A-C**). By ≥4 weeks post-transduction, CaCC current density
155 in ARB iPSC-RPE increased significantly, reaching levels comparable to WT iPSC-RPE (**Figures 2D, E**
156 **and S2E**). Furthermore, transduced monolayers of ARB iPSC-RPE demonstrated enhanced degradation
157 of rhodopsin following POS feeding (**Figure 2F and S2I**). These findings, together with those reported
158 by Guziewicz et al. (22) and Li et al. (23), support *hBEST1* gene augmentation as a treatment for ARB.
159
160 ***BEST1* augmentation restores CaCC activity and enhances rhodopsin degradation in R218C and**
161 **N296H adBD iPSC-RPE, but not in A146K adBD iPSC-RPE.**

Although not as intuitive, we suspected that gene augmentation might also be a viable solo therapeutic strategy for adBD-causing *BEST1* mutations. More specifically, we hypothesized that CaCC activity could be restored by increasing the intracellular ratio of wildtype to mutant BEST1 monomers available to form the homo-pentameric channel.

The same *hVMD2-hBEST1-T2A-GFP* lentiviral construct that was tested in ARB iPSC-RPE was used to transduce iPSC-RPE from all three adBD patients (**Figure S2D**). Following gene augmentation, BEST1 levels in each adBD iPSC-RPE model were comparable to those achieved in gene augmented ARB-iPSC-RPE and >3-fold higher than BEST1 levels present in parallel cultures of untreated adBD iPSC-RPE (**Figure 3A and S2C**). At ≥4 weeks post-transduction, CaCC activity was fully restored in the R218C and N296H adBD iPSC-RPE models, whereas the A146K adBD iPSC-RPE model remained unresponsive (**Figure 3B-D and S2F-H**) despite displaying the highest fold increase in BEST1 expression (**Figure 3A**). Consistent with these single-cell electrophysiological findings, gene augmentation improved rhodopsin degradation in R218C and N296H iPSC-RPE, but not in A146K iPSC-RPE (**Figure 3E and S2J-L**).

Gene editing specifically targets the mutant allele in A146K adBD iPSC-RPE and restores CaCC activity.

To determine whether A146K iPSC-RPE would respond to an alternative therapeutic approach, we tested gene editing as a means to eliminate expression of the mutant *BEST1* allele. Gene editing with CRISPR-Cas9 creates targeted double strand breaks in genomic DNA that are primarily repaired by endogenous non-homologous end joining (NHEJ) (26), leading to indels. These indels can cause transcriptional frameshifts that lead to premature termination codons, activation of intrinsic nonsense-mediated decay (NMD) pathways, and degradation of transcription products (27, 28).

An sgRNA sequence targeting specifically the A146K locus in the mutant *BEST1* allele was cloned into a lentiviral plasmid that encoded both the sgRNA (expressed via a U6 promoter) and a human codon optimized *Streptococcus pyogenes Cas9* (*spCas9)-T2A-GFP* transcript (expressed via a *hVMD2* promoter) (**Figures 4A and 4B**). We also cloned a sgRNA sequence targeting the *AAVS1* safe harbor locus (29) into the same lentiviral plasmid backbone to serve as an experimental control.

Two weeks after transduction of A146K adBD iPSC-RPE with A146K sgRNA or control (*AAVS1* sgRNA) lentiviral genome editor, we quantified the average frequency of deep sequencing reads corresponding to WT, mutant, and edited alleles in genomic DNA. We detected a nearly 80% editing frequency of the A146K mutant allele with no decrease in WT allele frequency post-editing (**Figure 4C**). Together, these results reflect efficient editing with high specificity for the A146K mutant allele over the WT *BEST1* allele.

Using deep sequencing, we next examined specific indels that were introduced into A146K iPSC-RPE two weeks post-transduction with the A146K sgRNA genome editor (**SI data file A**). An average of 95.4% of the edited alleles resulted in a frameshift mutation (**Figure 4D and SI data file A**), which is higher than the percentage of out-of-frame indels predicted by a recent machine learning algorithm (**SI data file A**) (30). This finding indicates a high likelihood that indels resulting from gene editing at the A146K locus in the mutant *BEST1* allele will trigger NMD of the transcribed RNA, effectively knocking out expression of the mutant allele in the vast majority of edited RPE cells.

We next assessed functional rescue of BEST1 channel activity in AAVS1 control versus A146K mutant allele gene-edited iPSC-RPE. Single-cell patch-clamp experiments revealed restoration of CaCC activity in gene-edited A146K iPSC-RPE, but not in control *AAVS1* sgRNA treated A146K iPSC-RPE (**Figure 4E, F and S3**).

Mutant allele-specific gene editing restores CaCC activity in all tested adBD iPSC-RPE.

While the gene editing results obtained in the A146K adBD iPSC-RPE model were highly encouraging, it is possible that this locus is unique in its potential to be targeted by a mutant allele-specific sgRNA. To extend this investigation, we also evaluated the specificity and efficacy of gene mutant allele editing in the N296H and R218C adBD iPSC-RPE models. N296H and R218C mutant allele-targeted sgRNAs were designed and cloned into separate lentiviral plasmids as described for the A146K sgRNA. N296H iPSC-RPE and R218C iPSC-RPE were transduced with lentiviral genome editors encoding either control (*AAVS1*) or corresponding allele-targeted sgRNA and editing outcomes were measured via deep sequencing of genomic DNA (**SI data file A**). Quantification of WT and mutant allele frequency revealed efficient targeting of the N296H and R218C mutant alleles with their respective sgRNAs (55.5% and 66.4%, respectively) with no demonstrable targeting of the WT alleles (**Figure 4G, I**). A high proportion of editing in these two models resulted in out-of-frame indels (96.0% and 94.5% for N296H and R218C iPSC-RPE, respectively) (**Figure 4H, J**). Subsequent single-cell patch-clamp measurements of CaCC current density confirmed restoration of channel activity post-gene editing in both R218C and N296H iPSC-RPE (**Figure 4K-M and S3).** Thus, while some variation in gene editing efficiency was observed using the three different sgRNAs (as expected), more than half of the mutant alleles were edited (with a high percentage of out-of-frame indels) in the three adBD iPSC-RPE models, with no editing of the WT allele.

Mutant allele-specific gene editing does not perturb global iPSC-RPE transcriptional programs, although off-target editing can occur.

Although the mutant allele-specific sgRNAs tested in the three adBD iPSC-RPE models did not target the fellow WT alleles in any of our experiments, the potential for off-target adverse effects

231 elsewhere within the genome still exists. To detect untoward transcriptional effects from gene editing, we
232 performed single-cell RNA sequencing (scRNA-seq) for 12,061 individual iPSC-RPE cells treated with
233 genome editors. iPSC-RPE (R218C, N296H, A146K, or isogenic control R218C>WT) were edited with
234 genome editors encoding either a mutant allele-targeted sgRNA or a control sgRNA targeting the *AAVS1*
235 site, to generate a total of eight separate samples (**Figure S4A**).

236 Evaluation of t-Distributed Stochastic Neighbor Embedding (t-SNE) clustering of cells across all
237 eight samples indicated that, by virtue of using the *hVMD2* promoter, *spCas9-T2A-GFP* transcript levels
238 closely corresponded with *BEST1* transcript levels (**Figure 5A**). Visual comparison of t-SNE clustering of
239 each individual sample demonstrated that transcriptional signatures are grossly similar between iPSC-
240 RPE lines, whether treated with mutant allele-targeted (+GE) or control (*AAVS1*) sgRNA (**Figure 5B**
241 ***top***). This observation was supported quantitatively by non-negative matrix factorization (NMF). NMF
242 analysis demonstrated that greater transcriptome variation exists between iPSC-RPE from different lines
243 than between iPSC-RPE from the same line treated with mutant allele-targeted or control sgRNA (**Figure**
244 **S4B**).

245 Additional analysis of global gene expression (**Figure 5B *bottom***) and of a focused set of genes
246 related to negative or off-target effects (including cell cycle regulation, apoptosis, DNA damage response,
247 or innate immune response; **Figure S4C, SI data file B**) did not reveal significant upregulation of those
248 gene sets in mutant allele-targeted (+GE) versus control sgRNA-treated samples. However, examination
249 of the top nine potential off-target sites for the R218C sgRNA revealed a low, yet significant percentage
250 of editing at a single site within a non-coding region of chromosome 7 (**Figure 5C**). While this finding is
251 not predicted to have a deleterious effect on RPE cell function, it emphasizes the importance of
252 performing comprehensive on- and off-target genome editing analyses using a patient-specific model
253 system.

Discussion

The observation that a subset of adBD mutations may be amenable to gene augmentation greatly expands the Best disease patient population that might benefit from this therapeutic approach. Based on the crystallographic studies by Dickson et al. (16), the two mutations that responded to gene augmentation lie within calcium clasp (N296H) or chloride binding (R218C) sites within the BEST1 channel, whereas the mutation that failed to respond (A146K) localizes to a putative structural region. Among the over 200 known *BEST1* mutations, many are predicted to be directly or indirectly involved in ion binding (16, 31). Importantly, a recent study by Ji et al. using baculovirus supports our finding that chloride and calcium binding site mutations in BEST1 can be receptive to gene augmentation (32). However, the fact that not all adBD iPSC-RPE models respond to gene augmentation underscores the need to vet patient candidacy for gene augmentation carefully.

The mechanism underlying selective responsivity of adBD patients to gene augmentation cannot be due to traditional allelic haploinsufficiency, in which half the normal amount of WT protein and no mutant protein is produced, resulting in fewer (but fully WT) BEST1 channels. Such a situation exists in parents of ARB patients, who have no demonstrable disease phenotype. Rather, adBD mutant monomers must be incorporated alongside WT monomers in all (or nearly all) BEST1 channels (33). We propose that in the case of N296H and R218C, this commingling of WT and mutant monomers causes ion binding site insufficiency and channel impermeability, a condition that is surmountable by WT *BEST1* augmentation. In contrast, we hypothesize that *BEST1* mutations like A146K—which converts a nonpolar amino acid to a polar amino acid in a compact structural region of the protein—has more pervasive functional consequences, resulting in greater resistance to gene augmentation.

We did consider the possibility that mutation-specific resistance to gene augmentation was due to variability in transgene expression (*i.e.*, there was insufficient WT transgene expression in the non-

277 responsive A146K adBD iPSC-RPE model). However, we found that BEST1 protein levels were similar
278 in all models following gene augmentation. In fact, a slightly higher fold-increase in BEST1 levels was
279 achieved in A146K adBD iPSC-RPE compared with the two adBD models that were rescued by gene
280 augmentation (N296H and R218C). Thus, it is highly unlikely that the differences in functional response
281 observed between R218C or N296H adBD iPSC-RPE and A146K adBD iPSC-RPE are due to variability
282 in transgene expression. Resistance of the A146K mutation to functional recovery after gene
283 augmentation also cannot be explained by occult artifacts inherent to the iPSC line or its RPE progeny,
284 since gene editing was ultimately successful in restoring CaCC activity in the same differentiated A146K
285 adBD iPSC-RPE population.

286 It is also notable that our lentiviral constructs employed the *hVMD2* promoter, which is ideal from
287 a translational standpoint as it specifies expression in RPE and supports native regulation of *BEST1*. Use
288 of alternative promoters poses risks of off-target cell effects and/or undesirably low (ineffectual) or high
289 (toxic) levels of protein expression. For construct delivery, we selected lentivirus based on its excellent *in*
290 *vitro* RPE transduction efficiency (17, 25) and its current use in RPE gene therapy trials
291 (ClinicalTrials.gov Identifiers: NCT01367444, NCT01736592) (24). However, our findings are likely
292 applicable across all *in vivo* transgene delivery platforms that possess comparable safety and transduction
293 efficiency profiles. Indeed, Ji et al. observed improvement in CaCC activity in isolated R218H adBD
294 iPSC-RPE cells following constitutive overexpression of WT BEST1 using an AAV delivery vector (32).

295 There is precedence for using patient-specific iPSCs as preclinical efficacy models for gene
296 therapy clinical trials (34). Our work extends this utility by providing a framework for preclinical testing
297 of mutation-specific responses in a genotypically heterogenous disease using the affected cell type. It
298 remains to be determined whether separate adBD iPSC-RPE models will be required to assess suitability

of gene augmentation versus gene editing for every mutation, or if a few models can sufficiently represent larger categories of mutations (*e.g.*, ion binding sites or structural regions) (35).

For adBD mutations like A146K that are not amenable to gene augmentation, we showed that targeted gene editing holds great promise as an alternative therapy. Indeed, there is a wide spectrum of *BEST1* mutations that could be treated by CRISPR-Cas9 by designing unique mutation-targeted sgRNAs (examples shown in **SI data file D**). While this approach would be costly and time-consuming if separate testing is required for each mutation-specific sgRNA, rapid advances in gene editing technologies and strategies may overcome such limitations. Other gene therapy strategies also exist for dominant ocular diseases; for example, knockdown of both wildtype and mutant allele transcripts with simultaneous introduction of a modified wildtype gene (36). Whether such an approach would be safe and effective for adBD mutations that fail to respond to straightforward gene augmentation is not known, but could be tested using the iPSC-RPE model systems employed here.

In our gene editing experiments, we observed higher efficiency out-of-frame editing in iPSC-RPE when compared to a prior study using undifferentiated iPSCs (19). This finding is consistent with recent reports of variable mutation bias across different cell types (30), and points to the importance of evaluating gene editing using the specific cell type(s) targeted by disease. In addition, editing at *BEST1* in iPSC-RPE did not provoke an increase in expression of genes associated with cell cycle regulation, apoptosis, DNA damage response, or innate immune response in comparison to editing at a well characterized safe-harbor locus (29) with a previously described sgRNA (37). Undesirable effects such as these have been reported in other cell types following Cas9-mediated gene editing (11, 38). Despite our reassuring findings, there remains the potential for off-target genomic alterations, as was observed at a single locus in a small percentage of iPSC-RPE cells in the R218C adBD model. While these particular off-target indels are in a non-coding region and are thus predicted to be functionally silent, their presence

emphasizes the value of employing human model systems for preclinical genome editing safety studies. Interestingly, no off-target indels were detected in our prior study using the same sgRNA in undifferentiated R218C iPSCs (19), which further indicates the need to perform off-target analyses in iPSC-RPE and not in surrogate cell types.

Overall, our results provide a blueprint to guide gene therapy choice in the era of gene augmentation and gene editing (**Figure 6**). With its inherently larger target populations and established track record in patients, it is practical to utilize gene augmentation when possible, reserving gene editing for mutations that require allele repair or knockout or are otherwise untreatable by gene augmentation. It is noteworthy that the two adBD lines that demonstrated restoration of CaCC activity with gene augmentation or gene editing did so with equal efficacy, underscoring the suitability of either approach. Other desirable characteristics of Best disease as a clinical candidate for gene therapy include 1) a wide time window for gene therapy intervention, 2) accessibility of RPE using standard surgical techniques, 3) a small (~5.5 mm diameter) treatment area, 4) availability of noninvasive retinal imaging and functional assessment tools, and 5) growing patient safety data from other RPE-based gene therapy trials (2-4). As such, Best disease is well-positioned to become the first genotypically heterogeneous disorder with dominant and recessive inheritance patterns to have a full menu of therapeutics for all affected individuals. Furthermore, implications of this work likely extend beyond the eye and Best disease to other intractable monogenic conditions caused by mutations in multimeric ion channels, including congenital myasthenic syndromes and some forms of epilepsy (39-41).

Acknowledgements

The authors thank Alfred Lewin (U. Florida) for the *hVMD2-hBEST1-T2A-GFP* plasmid construct; the Cellular Imaging and Analysis core at the University of Wisconsin-Madison Waisman Center; and

Andrew Thliveris for helpful discussions. This work was supported by NIH R01EY024588 (to D.M.G., B.A.T., and E.M.S.); Foundation Fighting Blindness, Research to Prevent Blindness, Retina Research Foundation Emmett Humble Chair, and McPherson Eye Research Institute Sandra Lemke Trout Chair in Eye Research (to D.M.G.); NSF CBET-1350178 and CBET-1645123, NIH R35GM119644, Brain & Behavior Research Foundation, Burroughs Wellcome Fund, and Retina Research Foundation Kathryn and Latimer Murfee Chair (to K.S.); NIH R01EY024995 and Retina Research Foundation M.D. Mathews Professorship (to B.R.P.); NIH T32HG002760 and F30EY027699, VitreoRetinal Surgery Foundation (to B.S.); DGE-1747503 (to K.M.). This study was supported in part by a core grant to the Waisman Center (NICHHD U54 HD090256). We thank members of the Gamm and Saha labs for comments on the manuscript, plasmid depositors to Addgene, the University of Wisconsin-Madison Biotechnology Center for DNA sequencing, and the University of Wisconsin-Madison Skin Disease Research Center for assistance with virus preparation.

Author contributions

D.S. and D.M.G. designed the gene augmentation experiments. B.S., D.S., D.M.G. and K.S. designed the gene editing experiments. P.K.S. and B.R.P. performed and analyzed the electrophysiology experiments. D.S. and B.S. performed all other experiments with contributions from R.V., K.L.E., C.B, S.S.S., A.A., and E.C. K.M., S.S., V.P., A.F.S., and S.R. were primarily responsible for the scRNA-seq analysis. B.A.T. and E.M.S. provided and characterized the ARB iPSC line, D.S., B.S., K.S., and D.M.G. wrote the manuscript and analyzed data with input from all authors. D.M.G., K.S., and B.R.P. supervised research.

Competing interests statement

The authors declare no competing interests.

Figures and legends

Figure 1

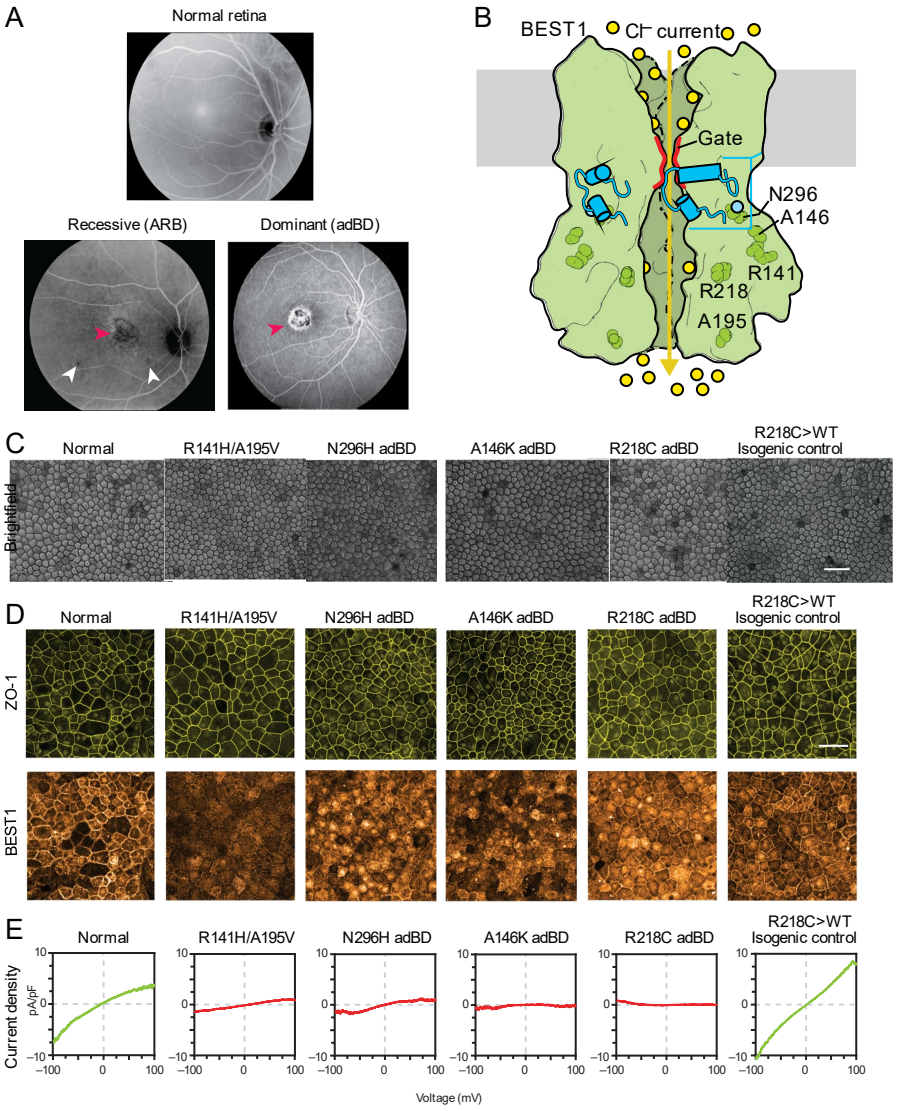

Figure 1 | *BEST1* mutations reduce CaCC current in Best disease iPSC-RPE. (A) *top*, image (in grayscale) of a normal fundus; *bottom left*, fundus image of an ARB patient with R141H/A195V compound heterozygous mutations in *BEST1* showing a vitelliform lesion in the macula (*red* arrowhead) as well as small lesions outside the macula (*white* arrowheads); *bottom right*, fundus image showing a vitelliform macular lesion (*red* arrowhead) in an adBD patient with a heterozygous R218C encoding mutation in *BEST1*. **(B)** A fully functional homo-pentameric BEST1 channel is formed by assembly of

377 WT subunits (*green*), allowing movement of chloride ions (*yellow* circles) upon binding of calcium ions
378 (*light blue* circle) (based on the eukaryotic Best1 crystal structure (16)). **(C)** Light microscopic images of
379 normal, patient-specific, and isogenic control iPSC-RPE used in this study. Scale bar = 50 µm (applies to
380 all images in C). **(D)** Immunocytochemical analyses of ZO-1 and BEST1 protein expression in iPSC-RPE
381 cells. Scale bar = 50 µm (applies to all images in D). **(E)** CaCC current density-voltage plots from WT,
382 R141H/A195V ARB, or adBD iPSC-RPE cells, as determined by calculating the difference in average
383 chloride currents in the presence or absence of calcium (Figure S1). For +calcium: n = 6 cells for WT, 12
384 cells for R141H/A195V ARB, 7 cells for N296H adBD, 5 cells for A146K adBD, 5 cells for R218C
385 adBD, and 10 cells for R218C>WT isogenic control; for no calcium: n = 8 cells for WT, 12 cells for
386 R141H/A195V ARB, 8 cells for N296H adBD, 7 cells for A146K adBD, 8 cells for R218C adBD, and 9
387 cells for R218C>WT isogenic control (data combined from at least two replicates).

Figure 2

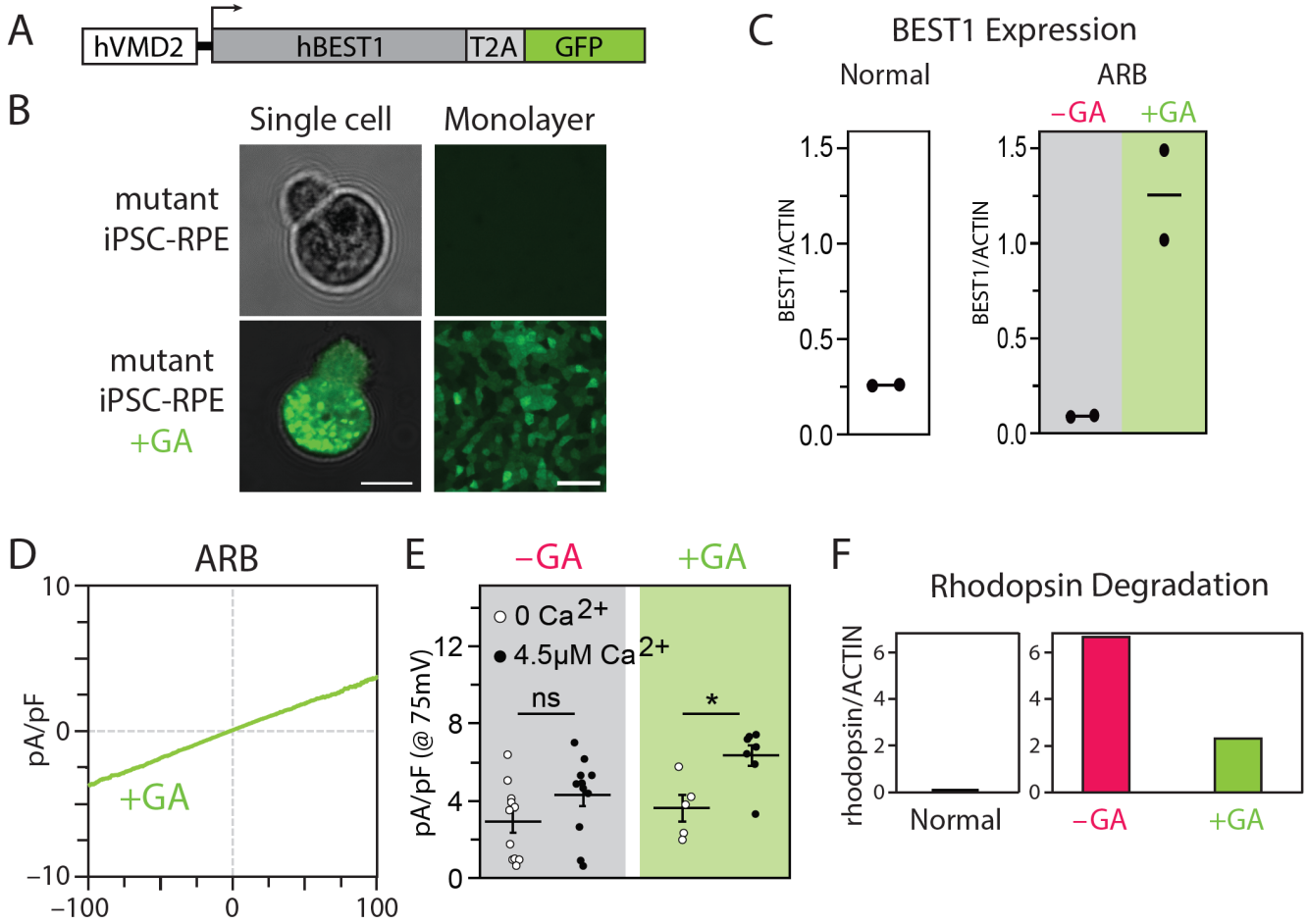

Figure 2 | Gene augmentation rescues the ARB iPSC-RPE cell phenotype. (A) Construct used for *BEST1* gene augmentation (GA). **(B)** Presence or absence of GFP fluorescence in a single dissociated iPSC-RPE cell (*left*) or iPSC-RPE monolayers (*right*) before (*top*) or after (*bottom*) gene augmentation. Scale bar = 10 μm (*left*); 50 μm (*right*). **(C)** Western blot-based quantification of BEST1 protein levels (normalized to ACTIN) in WT iPSC-RPE, ARB iPSC-RPE, and ARB iPSC-RPE after *BEST1* augmentation. **(D)** CaCC current density-voltage plots after gene augmentation in ARB iPSC-RPE. n = 7 cells for +calcium and 5 cells for no calcium (data combined from two replicates (Figure S2)). **(E)** CaCC conductance for individual ARB iPSC-RPE cells at 75 mV before or after gene augmentation. The

number of cells is the same as for panels 1E and 2D. Error bars represent mean ± SEM; ns = $p \geq 0.05$, * for $p < 0.05$. **(F)** Western blot-based quantification of rhodopsin levels 120 hr after photoreceptor outer segment (POS) feeding in WT iPSC-RPE or in ARB iPSC-RPE with or without WT *BEST1* gene augmentation.

Figure 3

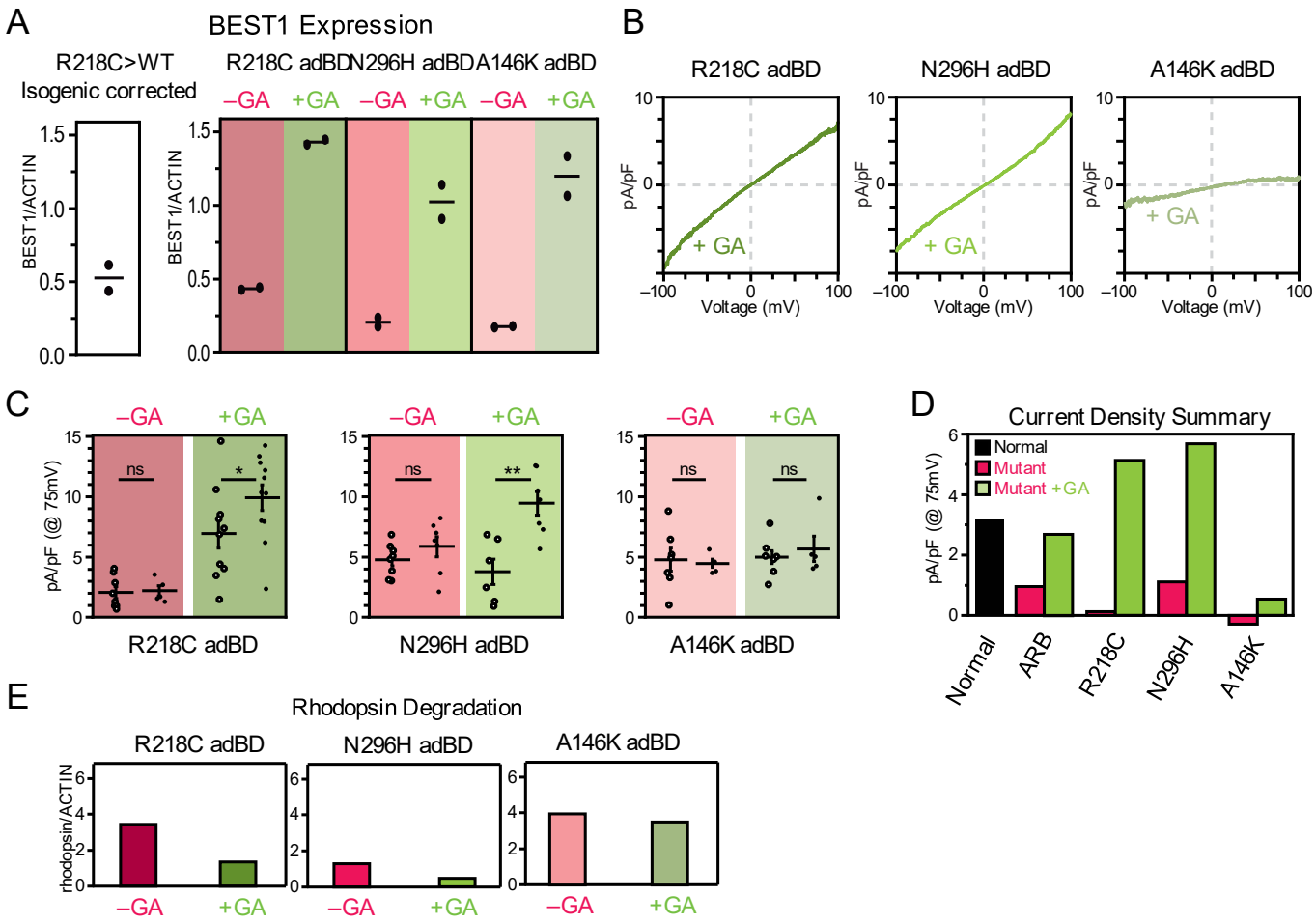

Figure 3 | Gene augmentation rescues the cell phenotype in some, but not all, adBD iPSC-RPE models. (A) Western blot-based quantification of BEST1 protein levels (normalized to ACTIN) in WT iPSC-RPE and in the adBD iPSC-RPE models before and after *BEST1* gene augmentation (GA). **(B)** CaCC current density-voltage plots after gene augmentation in adBD iPSC-RPE. For +calcium: n = 11 cells for R218C, 7 cells for N296H, and 5 cells for A146K; for no calcium: n = 9 cells for R218C, 6 cells for N296H, and 8 cells for A146K (data combined from two replicates). **(C)** CaCC conductance for individual adBD iPSC-RPE cells at 75 mV before and after gene augmentation. The number of cells is the same as for panels 1E and 3B. Error bars represent mean ± SEM; ns = $p \geq 0.05$, * for $p < 0.05$, ** for p

413 <0.01. **(D)** Mean CaCC conductance at 75 mV before or after gene augmentation for all iPSC-RPE tested.

414 **(E)** Rhodopsin levels 48 hours after feeding POS to adBD iPSC-RPE with or without WT *BEST1* gene

415 augmentation.

416

417

418

419

420

421

422

423

424

425

426

427

428

429

430

431

432

433

Figure 4

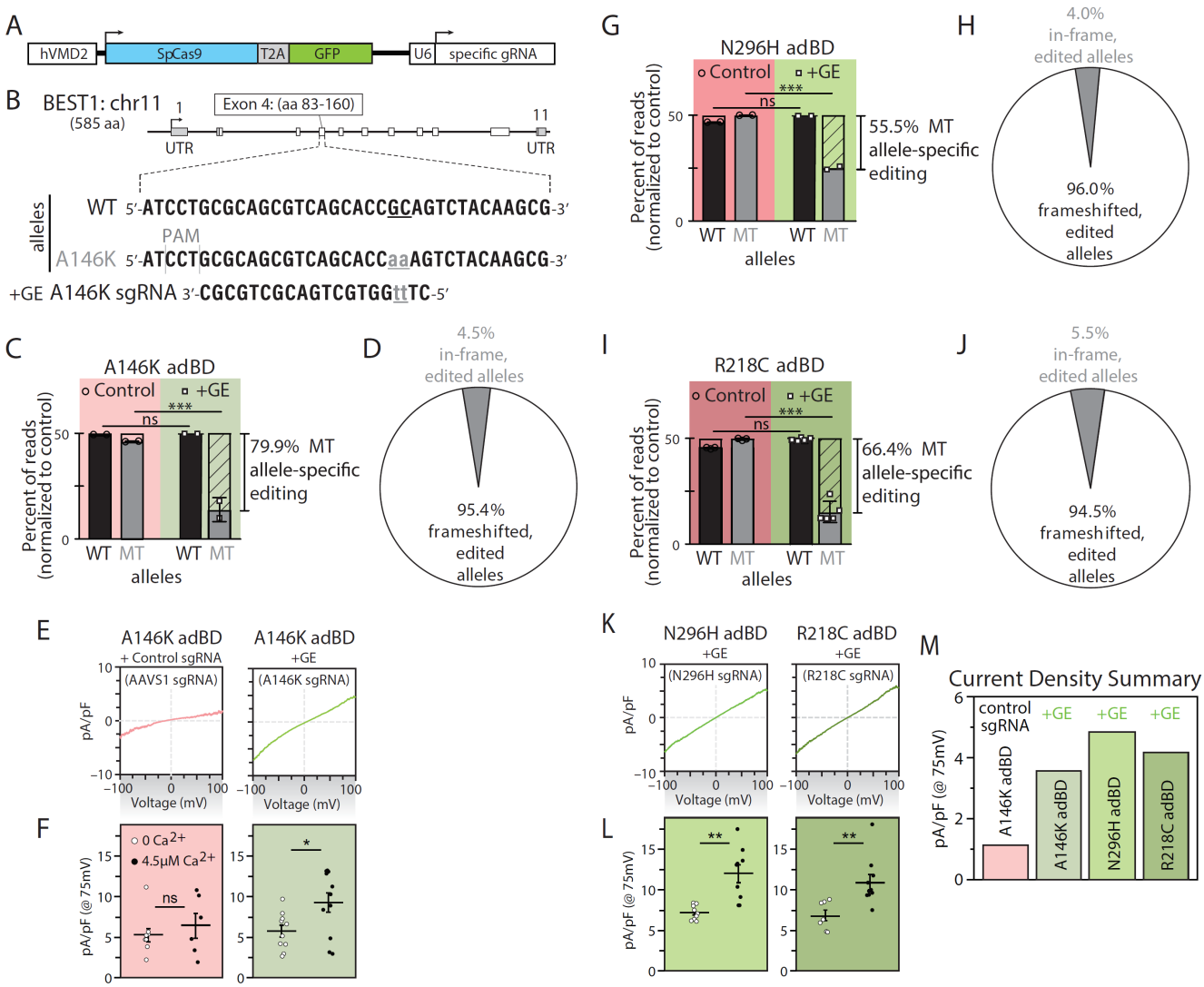

Figure 4 | Gene editing specifically and efficiently introduces frameshifts within the mutant allele in adBD iPSC-RPE and rescues CaCC activity. (A) Lentiviral genome editing construct expressing *sp*Cas9 and mutant allele-targeted sgRNAs. **(B)** Diagram showing the heterozygous base pair substitutions in A146K adBD and the design of the A146K sgRNA. The wildtype (WT) allele is shown above, while the A146K adBD allele is shown below, with the mutated bases indicated in lower case and underlined. **(C)** Percentage of WT and mutant (MT; unedited and edited) allele sequencing reads in A146K iPSC-RPE treated with A146K sgRNA lentiviral genome editor ("+GE"), respectively,

443 normalized to control ("Control", genome edited with safe harbor *AAVS1*-targeting sgRNA). **(D)** Indel
444 frameshift and in-frame frequency for mutant allele-edited reads from A146K adBD iPSC-RPE
445 (corresponds to 4C). **(E)** CaCC current density-voltage plots and **(F)** CaCC conductance for individual
446 iPSC-RPE cells from single-cell patch clamp experiments for A146K iPSC-RPE treated with control
447 (*AAVS1*) or mutant allele-targeted sgRNA lentiviral genome editor. **(G-J)** Percentage of WT and mutant
448 (MT; unedited and edited) allele sequencing reads in N296H (G) or R218C (I) adBD iPSC-RPE treated
449 with N296H or R218C sgRNA lentiviral genome editor, respectively, normalized to control (*AAVS1*
450 sgRNA). Indel frameshift and in-frame frequency in N296H (H) or R218C (J) adBD iPSC-RPE treated
451 with N296H or R218C sgRNA lentiviral genome editor, respectively (correspond to 4G and 4I,
452 respectively). **(K)** CaCC current density-voltage plots and **(L)** CaCC conductance for individual iPSC-
453 RPE cells from single-cell patch clamp experiments for N296H or R218C adBD iPSC-RPE treated with
454 respective mutant allele-targeted sgRNA lentiviral genome editor. **(M)** Mean CaCC conductance at 75
455 mV for each adBD iPSC-RPE model. The number of cells is the same as 4E and 4K. For gene editing
456 experiments (4C,D and G-J), n = 2 (A146K IPSC-RPE and N296H RPE) and n = 5 (R218C iPSC-RPE).
457 For electrophysiology experiments (4E,F and K-M), +calcium: n = 6 cells for *AAVS1*, 11 cells for A146K,
458 9 cells for N296H, 10 cells for R218C; no calcium: n = 9 cells for *AAVS1*, 10 cells for A146K, 9 cells for
459 N296H, 7 cells for R218C (data combined from two replicates). Error bars in 4C,G,I represent mean ±
460 SD; ns = $p \geq 0.05$, *** for $p < 0.001$. Error bars in 4F and 4L represent mean ± SEM; ns = $p \geq 0.05$, * for p
461 < 0.05, ** for $p < 0.01$.
462
463
464
465

Figure 5

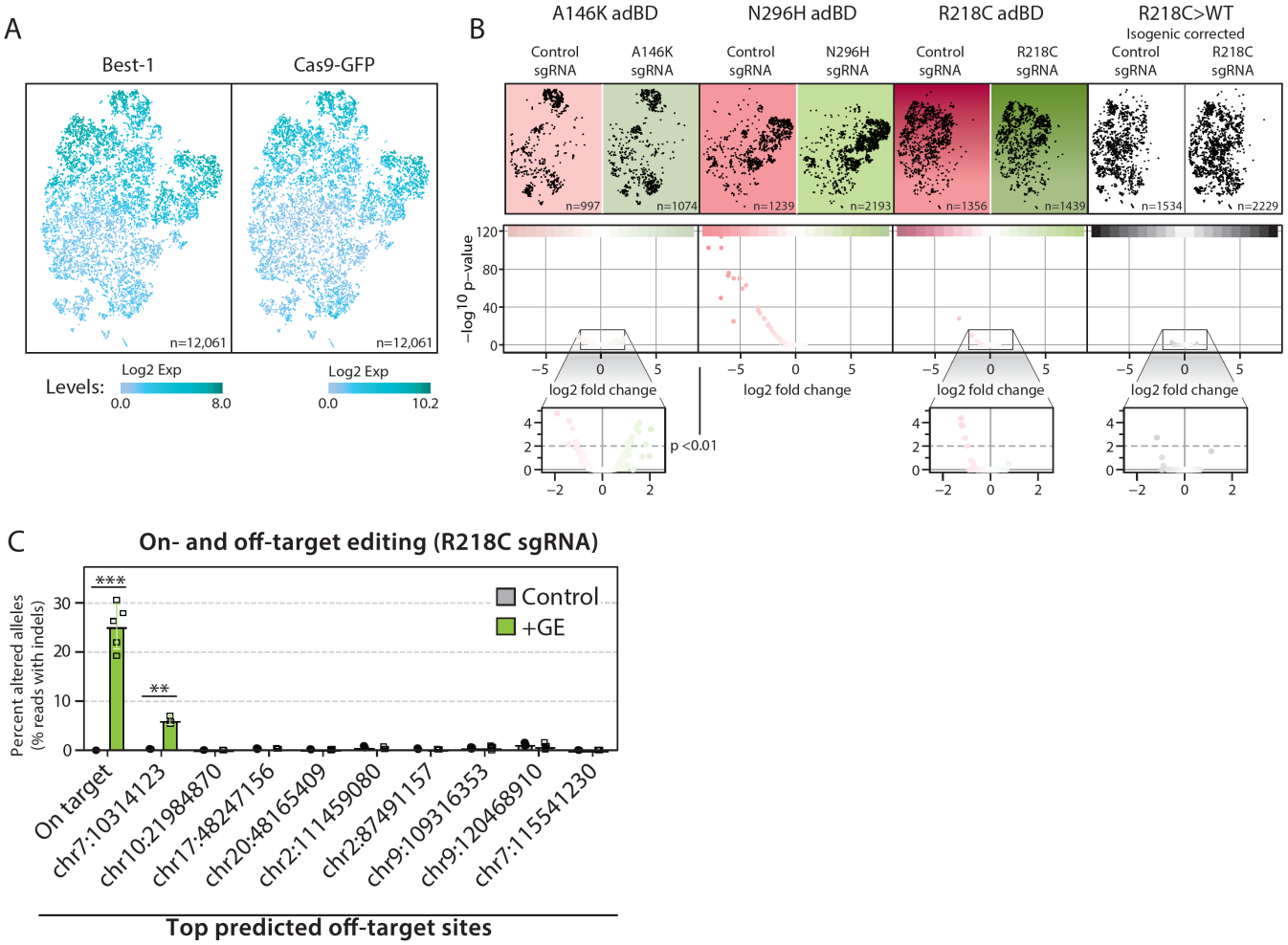

Figure 5 | Gene editing did not disrupt iPSC-RPE transcriptional programs. (A) t-SNE plot of single iPSC-RPE cells across all 8 samples with relative expression of *BEST1* (*left*) and *spCas9-T2A-GFP* (*right*) depicted via increasing shades of *blue*. Total number of cells analyzed (n) is shown. **(B)** *Top*, t-SNE plot of single cells (*black* dots) from each treated sample. Number of cells analyzed (n) for each sample is shown. *Bottom*, Volcano plots of transcriptome-wide differences in expression of individual genes (*red* or *green* dots) between iPSC-RPE of the same genotype treated with mutant allele-targeted sgRNA (*green*) versus control (*AAVS1*, *red*) sgRNA lentiviral genome editor. p <0.01 was the threshold

476 for determining significant versus non-significant changes in gene expression. **(C)** Frequency of edited
477 alleles at on-target and top nine ranked off-target loci in R218C adBD iPSC-RPE treated with R218C
478 sgRNA lentiviral genome editor (n=3 for control and n=5 for +GE, except n=3 at first *chr 7* off-target
479 locus). Off-target sites are annotated by the location of the first base of the predicted off-target site
480 (further detailed in SI Data File C). Error bars represent mean ± SD; ** for $p < 0.01$, *** for $p < 0.001$.
481
482
483
484
485
486
487
488
489
490
491
492
493
494
495
496

497 **Figure 6**

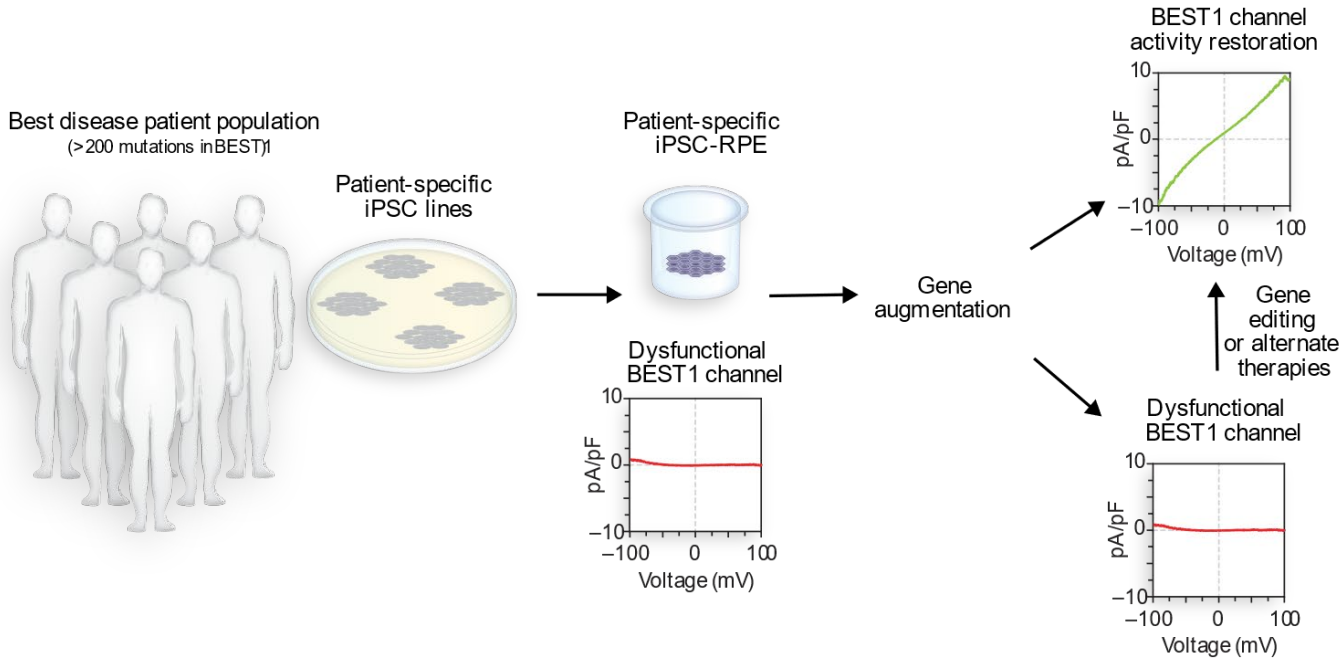

498

499

500 **Figure 6 | In vitro gene therapy testing strategy for adBD.** The amenability of adBD mutations to
501 correction via gene augmentation can be evaluated for efficacy and safety in a dish using patient iPSC-
502 RPE models. Those patients with mutations that fail to respond to gene augmentation would then undergo
503 further testing for genome editing (or another alternative strategy) using the same adBD iPSC-RPE model
504 systems.

Materials and Methods

iPSC lines

A total of 6 iPSC lines, 2 control and 4 patient-specific, were used in this study. In addition to one control iPSC line (normal) and two adBD patient-specific iPSC lines (A146K adBD and N296H adBD) previously used by our group for Best disease modeling (17), we used three new iPSC lines. Two of the new iPSC lines harbored patient specific mutations: R218C for adBD and R141H/A195V for ARB. One isogenic control iPSC line was obtained by CRISPR/Cas9-based gene correction of the patient-specific R218C adBD iPSC line (19). All iPSC lines were cultured either on mouse embryonic fibroblasts (MEFs) or on Matrigel. Lines cultured on MEFs were maintained using iPS media (Dulbecco's Modified Eagle's Medium (DMEM)/F12 (1:1), 20% Knockout Serum Replacement (KOSR), 1% MEM non-essential amino acids, 1% L-glutamine, 0.2 mM β-mercaptoethanol, 100 ng/ml FGF-2), and iPSCs cultured on Matrigel were cultured with either mTeSR1 or StemFlex media. MEFs, FGF-2, and Matrigel were purchased from WiCell (Madison, WI). All other cell culture reagents were purchased from ThermoFisher Scientific. Karyotype analysis was performed as a quality control. The manuscript does not contain human subject or animal studies, and all work with iPSC lines was carried out in accordance with institutional, national, and international guidelines and approved by the Stem Cell Research Oversight Committee at the University of Wisconsin-Madison.

Differentiation of iPSC lines to RPE

Differentiation of iPSCs to RPE was performed as previously described (17, 42). Briefly, iPSCs were enzymatically lifted (1 mg/ml dispase for cells cultured on MEFs; 2 mg/ml dispase or 1 ml ReLeSR for cells cultured on Matrigel) to form aggregates, also referred to as embryoid bodies (EBs). EBs were maintained in suspension culture either in EB media (iPS media without FGF-2) and then switched to

528 neural induction media (NIM) on day 4, or gradually weaned off mTeSR1/StemFlex and transitioned to
529 NIM by day 4. NIM is composed of 500 ml DMEM/F12 (1:1), 1% N2 supplement, 1% MEM non-
530 essential amino acids, 1% L-glutamine, 2 µg/ml heparin. EBs were plated on laminin (Cat# 23017015)
531 coated 6-well plates (Nunc; Thermo Fisher Scientific) on day 7. On day 16, neural rosettes were
532 mechanically lifted, leaving adherent cells behind that were maintained in retinal differentiation media
533 (RDM; DMEM:F12 (3:1), 2% B27 without retinoic acid, 1% antibiotic-antimycotic solution). For the first
534 four media changes, RDM was supplemented with 10 µM SU5402 and 3 µM CHIR99021.
535 After 60 days of differentiation, pigmented patches of RPE were micro-dissected, dissociated
536 using Trypsin-EDTA (0.25%), and plated on laminin coated surfaces in RDM with 10% FBS and Rho
537 kinase inhibitor (ROCKi; Y-27632). After 2 days, the media was changed to RDM with 2% FBS, and
538 eventually to RDM once the cells were fully confluent. There were no differences observed between RPE
539 differentiated from iPSCs cultured on MEFs and Matrigel. Mutant and wildtype genotypes of iPSC-RPE
540 were verified by Sanger sequencing periodically. Heparin (Cat# H-3149) and SU5402 (Cat# SML0443-
541 25MG) were from Sigma-Aldrich, CHIR99021 (Cat# 4423) was from Tocris Bioscience, and ReLeSR
542 was purchased from STEMCELL Technologies. All other differentiation reagents were purchased from
543 ThermoFisher Scientific.
544
545 **Gene expression analysis**
546 Reverse transcriptase-PCR was used to assess RPE-specific gene expression in RPE derived from
547 different iPSC lines, as described previously (17). Primers used are listed in Table S1.
548
549 **Generation of lentiviral vectors**

Lentiviral plasmid with the human *VMD2* promoter driving expression of *hBEST1-T2A-GFP* was provided by Alfred S. Lewin (University of Florida). LentiCRISPR v2 (LCv2) plasmid was purchased from Addgene (Cat# 52961). Lentiviral gene editing plasmids containing specific sgRNA sequences and the human *VMD2* promoter driving expression of *spCas9-T2A-GFP* were then generated as described hereafter (all primers and sgRNA sequences are listed in SI Tables). To begin, the '*T2A-GFP-WPRE*' sequence was amplified from the *hVMD2-hBEST1-T2A-GFP* plasmid using LCv2-GFP.Gib.F and .R primers and Q5 2X MM (NEB, Cat# M0492L). The '*2A-Puro-WPRE*' sequence was then removed from the LCv2 plasmid via restriction digestion with PmeI (NEB, Cat# R0560S) and BamHI (NEB, Cat# R3136S). The digestion product was resolved on a 0.7% agarose gel and the plasmid backbone was purified using the Monarch gel purification kit (NEB, Cat# T1020S). The '*T2A-GFP-WPRE*' sequence was inserted into the digested backbone using the Gibson Assembly kit (SGI, Cat# GA1100) per the manufacturer's instructions. The completed Gibson Assembly reaction was then amplified using chemically competent *E. coli* (NEB, Cat# C3040H) and Sanger sequenced to confirm insertion of '*T2A-GFP-WPRE*' using LCv2-GFP.seq.L and LCv2-GFP.seq.R primers. This intermediate plasmid product (*pLCv2-GFP*) was digested with AfeI (NEB, Cat# R0652S) and EcoRI-HF (NEB, Cat R310S) to remove the constitutive EF-1 alpha core promoter. The desired digestion product was purified as described above. The *hVMD2* promoter was then PCR amplified from *hVMD2-hBEST1-T2A-GFP* using Q5 2X MM and VMD2.LCv2.GFP.Gib.F and .R primers, followed by insertion into the digested LCv2-GFP backbone via Gibson Assembly. Next, the completed Gibson reaction was transformed into chemically competent *E. coli* and the sequence of the final product *hVMD2-spCas9-T2A-GFP* was confirmed via Sanger sequencing using VMD2.LCv2.GFP.seq.L and .R primers. Subsequently, specific sgRNAs were cloned into *hVMD2-spCas9-T2A-GFP* using the restriction digest and Gibson Assembly protocol.

Lentivirus production and cell transduction

Lentivirus stocks were generated by the Cell Culture Core of the UW Department of Dermatology Skin Disease Research Center (Madison, WI). Briefly, HEK293 cells cultured on 10-cm dishes were transfected with lentiviral plasmids—10 µg of sgRNA encoding lentiviral plasmid (*hVMD2-hBEST1-T2A-GFP or hVMD2-spCas9-T2A-GFP*); 5 µg of psPax2 (Addgene, Cat# 12260), and 2 µg of pMD2.G (Addgene, Cat# 12259)—using Lipofectamine (ThermoFisher; Cat# 11668019). After 15 hours, culture medium (DMEM with 10% FBS) was replaced with fresh media containing 1% Penicillin-Streptomycin. Media containing lentiviruses was collected the next day and viral titers were calculated using QuickTiter Lentivirus Titer Kit (Cell Biolabs, Cat# VPK-107). Titers for lentiviral stock were:

Lentivirus	**Titer (Transduction units/ml)**
hVMD2-hBEST1-T2A-GFP	$22x10^{6-7}$
hVMD2-spCas9-T2A-GFP R218C sgRNA	$74.16\ x10^{6-7}$
hVMD2-spCas9-T2A-GFP A146K sgRNA	$74.26\ x10^{6-7}$
hVMD2-spCas9-T2A-GFP N296H sgRNA	$68.91\ x10^{6-7}$
hVMD2-spCas9-T2A-GFP AAVS1 sgRNA	$74.01\ x10^{6-7}$

For iPSC-RPE transduction, monolayers of iPSC-RPE on transwells were treated with 0, 5, 50, or 150 µl (Figure S3) or 150 µl alone of specified lentivirus preparation for all other experiments. Media was changed on day 2 to RDM, and cells were maintained in culture with media changes every 3 days until used for sequencing or other analyses.

Transepithelial electrical resistance (TER) measurements

Monolayers of RPE cultured on transwell inserts (Corning, #3470) were used for all TER measurements. To perform the measurements, we employed an epithelial voltohmmeter (EVOM2) with chopstick electrodes (STX2) from World Precision Instruments (Sarasota, USA) according to

591 manufacturer's instructions. Electrodes were sterilized with ethanol, and then rinsed in sterile Milli-Q
592 water followed by HBSS before measuring electrical resistance of RPE monolayers. Differences between
593 TER values of transwells with cultured RPE monolayers versus background measurements of cell-free
594 transwell inserts were multiplied by the surface area of the transwell membrane to obtain net TER values
595 in $\Omega \cdot cm^2$.
596
597 **Calcium-activated chloride channel current density measurements**
598 All iPSC-RPE cells used for chloride current measurements were cultured as a monolayer on
599 transwells. To singularize cells prior to measurement, transwells were washed twice with 0 Na-CMF
600 solution (135 mM N-Methyl-D-glucamine (NMDG)-Cl, 5 mM KCl, 10 mM HEPES, 10 mM glucose, 2
601 mM EDTA-KOH, pH adjusted to 7.4) and then incubated with papain enzyme solution (0 Na-CMF
602 solution containing 2.5 µl/ml papain (46 mg/ml, MP Biomedicals LLC, Cat#100921), 0.375 mg/ml
603 adenosine, 0.3mg/ml L-cysteine, 0.25 mg/ml L- glutathione, and 0.05mg/ ml taurine) for 30 minutes at
604 37ºC/5% CO_2. To stop the reaction, 0.01% BSA was added to the enzymatic solution. After washing
605 twice with 0 Na-CMF solution, cells were dispersed in extracellular solution containing 140 mM NaCl, 10
606 mM HEPES, 3 mM KCl, 2 mM $CaCl_2$, 2 mM $MgCl_2$, and 5.5 mM glucose adjusted to pH 7.4 with NaOH
607 by gentle pipetting.
608 Cells with polarized RPE morphology post-dissociation (Figure 2B, *left*) were used to measure
609 chloride currents. To test effects of gene augmentation or gene editing on *BEST1* mutant iPSC-RPE by
610 single-cell patch clamp analysis, only cells with GFP fluorescence (from transduction with *hVMD2-*
611 *hBEST1-T2A-GFP* for gene augmentation or *hVMD2-spCas9-T2A-GFP* encoding *AAVS1* sgRNA or
612 mutant allele-targeted sgRNAs for gene editing) were used. Current recordings on these cells were
613 performed using the conventional whole-cell patch clamp technique with an Axopatch 200A amplifier

614 controlled by Clampex software program via the digidata 1550 data acquisition system (Axon
615 Instruments, CA). Fire-polished borosilicate glass pipettes with 3-5 MΩ resistance were filled with pipette
616 solution containing 4.5 µM calcium or no calcium.
617 Recordings were carried out at room temperature and current-voltage tracings were established
618 using ramps from -100 to +100 mV for 1000 ms. The pipette solution with calcium was comprised of (in
619 mM) 146 CsCl, 5 (Ca^{2+})-EGTA-NMDG, 2 $MgCl_2$, 8 HEPES, and 10 sucrose at pH 7.3, adjusted with
620 NMDG. Another pipette solution devoid of calcium was comprised of (in mM) 146 CsCl, 5 EGTA-
621 NMDG, 2 $MgCl_2$, 8 HEPES, and 10 Sucrose at pH 7.3, adjusted with NMDG. Both of these pipette
622 solutions were mixed to make the solution containing 4.5 µM free calcium as described previously(43),
623 which was then used for patch clamping.
624 Current density values were obtained by dividing current amplitude with cell capacitance
625 measurements. CaCC current densities for iPSC-RPE are represented as differences between mean 4.5
626 µM calcium response and mean no calcium response from a total of at least five cells for each condition.
627 At least two differentiations were used as replicates to obtain data for each line.
628
629 **Immunocytochemistry**
630 iPSC-RPE cultured on transwell inserts were washed with PBS and fixed with 4%
631 paraformaldehyde for 10 minutes at room temperature (RT). After washing fixed cells three times with
632 PBS, transwell membranes were placed in blocking solution (10% normal donkey serum with 5% BSA,
633 1% fish gelatin and 0.5% Triton-X100 in PBS) for one hour at RT, and then incubated overnight at 4 ºC
634 in primary antibody (1:100 mouse anti-Bestrophin (Millipore, Cat# MAB5466); 1:100 rabbit anti-ZO-1
635 (ThermoFisher Scientific, Cat# 61-7300)) prepared in blocking solution. Cells were then washed three
636 times in PBS and incubated for 30 minutes at RT in appropriate secondary antibody (ThermoFisher

637 Scientific; 1:500 Donkey anti-Mouse IgG (Cat# A31571); 1:500 Donkey anti-Rabbit IgG (Cat# A10040))
638 prepared in blocking solution. Cells were again washed three times in PBS, incubated in DAPI (1:500;
639 ThermoFisher; Cat# D1306) for 30 minutes, mounted using prolong gold with DAPI (ThermoFisher; Cat#
640 P36931), and imaged using Nikon A1R confocal microscope with NIS Elements AR 5.0 software.
641
642 **Rhodopsin degradation assay**
643 Photoreceptor outer segment (POS) feeding of iPSC-RPE was performed as described previously (17).
644 Briefly, bovine POS (InVision BioResources (Seattle, WA)) were gently resuspended in DMEM. 100 µl
645 media was then removed from each transwell insert, $6.25x10^6$ POS were added, and cells were incubated
646 at 37 ºC and 5% CO_2 for 2 hours. Afterward, POS containing RDM was removed and each transwell was
647 washed thoroughly three times using DPBS. Following the washes, cells were harvested (0 time point) or
648 further incubated in fresh RDM for prescribed periods of time. At each time point, transwells were
649 washed, 100 µl RIPA buffer (ThermoFisher; Cat# 89900) containing protease inhibitor cocktail (Sigma-
650 Aldrich; Cat# P8340) was added, and cells were incubated on ice for 30 minutes to extract total cell
651 protein. Protein quantification was performed using the DC Protein assay kit II (Bio-Rad, Cat# 5000112).
652 Western blots were then performed to monitor rhodopsin degradation as described (17, 18).
653 Briefly, protein lysates were denatured in 1X Laemmli buffer (reducing) and kept on ice for 10 minutes.
654 Protein samples were then separated on 4-20% mini-Protean TGX gels (Bio-Rad; Cat# 4568095) and
655 electroblotted onto PVDF membranes (Millipore; IPFL10100). After blotting, membranes were dried at
656 RT for 15 minutes, re-activated in methanol for 1 minute, and then incubated in blocking buffer (1:1
657 Odyssey blocking buffer (LI-COR Biosciences; Cat# 927-40000):PBS) for 1 hour. Post-blocking, blots
658 were incubated in primary antibodies (1:500 mouse anti-rhodopsin (Millipore, Cat# MABN15); 0.1 µg/ml
659 rabbit anti-beta actin (Abcam, Cat# ab8227)) in blocking buffer with 0.1% Tween-20 overnight, washed

three times for 5 minutes each in PBS with 0.1% Tween-20, incubated for 1.5 hours at RT in appropriate secondary antibody (LI-COR Biosciences; 1:20,000 Donkey anti-Rabbit IgG (Cat# 926-32213); 1:20,000 Donkey anti-Mouse IgG (Cat# 926-68022)) in blocking buffer with 0.1% Tween-20 and 0.01% SDS, and then washed three times for 5 minutes each in PBS with 0.1% Tween-20. An Odyssey infrared Imager (LI-COR Biosciences) was used to image blots using Image Studio software. ImageJ was used for quantification of relevant protein bands. Samples from rhodopsin degradation assays were also used to assess levels of BEST1 protein before and after gene augmentation. Western blots were performed as described above, using 1:1000 rabbit anti-Bestrophin1 antibody (LAgen Laboratories; Cat# 016-Best1-01) and 1:1000 mouse anti-Actin antibody (Millipore; Cat# MAB1501) as primary antibodies.

Deep sequencing analysis of DNA and RNA read frequency

Cells were singularized with TrypLE Express (Gibco, Cat# 12605010) per manufacturer's instructions. Total DNA and/or RNA was extracted using QuickExtract DNA (Epicentre, Cat# QE09050) or QuickExtract RNA (Epicentre, Cat# QER090150), respectively. Both DNA and RNA extractions were performed per manufacturer's instructions with the following minor modifications: 1) a ratio of 10,000-25,000 cells per 50 µl of QuickExtract solution was routinely used, and 2) an optional DNase 1 treatment was omitted from the RNA extraction protocol. All samples were stored at -80 ºC until use.

RNA was reverse transcribed to cDNA using the ProtoScript II First Strand synthesis kit (NEB, Cat# E6560S) and synthesis was performed with the "random primer" option included within the kit. 4 µl of crude RNA extract was added to each cDNA reaction.

In preparation for targeted deep sequencing, Illumina adapter sequences and sample-specific barcodes were appended to genomic or cDNA amplicons via overhang PCR as described (19). Purified amplicon libraries were assembled into 2 nM total DNA in DNAse/RNAse free H_2O and sequenced using

683 150 nucleotide paired end reads using MiSeq (6M or 15M total reads) at the UW Biotech Center
684 (Madison, WI) with the following loading condition: 8 pmol total DNA and 15% PhiX DNA. Raw
685 FASTQ files were read and aligned to expected amplicons using a command line implementation of
686 CRISPResso (v1.0.8) (44). Full commands used for analysis are available upon request. 'Percent allele
687 identity' or 'percent edited' were determined using the software's standard output table of individual read
688 identities. Sequencing reads with counts <100 were not included in the analysis. All FASTQ files are
689 available upon request.
690
691 **Single-cell RNA sequencing (scRNA-seq)**
692 iPSC-RPE cultures derived from the A146K, N296H, and R218C adBD patient lines, and from an
693 isogenic gene-corrected control line derived from the R218C line (R218C>WT) were transduced with 150
694 µl of *hVMD2-spCas9-T2A-GFP* encoding specific sgRNAs as described in the 'Lentivirus production
695 and cell transduction' section. For each sample, sgRNAs were either targeted to mutant *BEST1* or to the
696 *AAVS1* locus (control). On day 14, cells were dissociated from transwells with a papain dissociation kit
697 (Worthington Biochemical, Cat# LK003150) and filtered using a Flowmi cell strainer (Bel-Art SP
698 Scienceware, Cat# H13680-0040) to obtain single-cell suspension. Cells were then prepared for scRNA-
699 seq with the droplet-based 10X Genomics GemCode platform according to the manufacturer's
700 instructions. In brief, singularized cells were encapsulated in oil beads containing a unique molecular
701 identifier (UMI) barcode. The cells were then lysed and cDNA libraries were created featuring cell and
702 transcript-specific molecular identifiers. Libraries were sequenced using an Illumina HiSeq2500 Rapid
703 Run and reads were aligned to a custom reference genome consisting of the human hg19 GRCh38
704 genome and an added gene for the *spCas9-T2A-GFP* transcript.
705

706 **scRNA-seq data analysis**

707 Gene edited iPSC-RPE were clustered based on their genome-wide transcriptome using the t-
708 Distributed Stochastic Neighbor Embedding (t-SNE) algorithm with the 10X Genomics Loupe Cell
709 Browser software (v2.0.0). Reads for each pair of samples (*BEST1* mutant allele-targeted sgRNA vs
710 *AAVS1* sgRNA control) were aligned, analyzed, clustered with Cell Ranger v2.1.1, and compared to
711 detect significant differences in gene expression, with p values adjusted using the Benjamini-Hochberg
712 correction for multiple tests. P <0.01 was used as the significance threshold for all analyses. Cell Ranger
713 using the aggregate feature was run to concatenate each pair of samples with the same genotype, and
714 differential gene expression within each pair (with gene editing at either the *AAVS1* or *BEST1* locus) was then
715 analyzed. Potential adverse events were probed using gene lists curated from gene ontology terms
716 associated with the cell cycle, apoptosis, DNA damage response, and the innate immune response, as well
717 as a list of 149 validated marker genes associated with human RPE (45) (**SI data file B**; gene ontology
718 sets are available on the Molecular Signatures Database
719 <http://software.broadinstitute.org/gsea/msigdb>). Differentially-expressed genes with p <0.01 were
720 deemed to be significant. All significantly differentially-expressed genes per cluster are reported, with the
721 exception of genes identified by Cell Ranger as having low average UMI counts. Volcano plots were generated
722 in RStudio (v.1.1.456) using the ggplot2 package.

723

724 **Non-negative matrix factorization-based comparison of scRNA-seq datasets**

725 Non-negative matrix factorization (NMF) followed by clustering of genes using the NMF factors was
726 used for Figure S4 to project each dataset into a gene group. The input data for this analysis were a set of gene
727 barcode matrices generated using the Cell Ranger 2.1.1 algorithm. The matrices were filtered to remove

728 background barcodes in order to include only detected cellular barcodes, and then further filtered to exclude
729 cells expressing fewer than 2000 total counts, followed by depth normalization.

730 To enable comparison of transcriptional signatures from each sample, NMF (46) was applied to
731 each scRNA-seq dataset. NMF is a popular dimensionality reduction and clustering approach that is used
732 to project data into low dimensional non-negative factors, and thus can be used to derive a clustering of
733 cells and genes. NMF with k=10 factors was applied with a total of five NMF runs. Next, the similarity of
734 NMF results was compared between two samples using the average best Jaccard coefficient between
735 clusters of one versus another sample. 1-average Jaccard coefficient was then used as the distance to
736 apply hierarchical clustering on the samples. This procedure was repeated five times and the tree that
737 appeared most often was used. The trees learned in different iterations were largely similar and always
738 grouped the patient-specific lines first before grouping different lines together.
739
740 **Quantification and statistical analysis**
741 Unless otherwise specified, all analyses were performed using GraphPad Prism (v.8.0.1) and error
742 bars represent mean ± SD; ns = $p \geq 0.05$, * for $p < 0.05$, ** for $p < 0.01$, *** for $p < 0.001$, **** for p
743 < 0.0001. Further detail for each analysis is provided here. Statistical analyses for Figures 2E, 2I and 4B
744 were performed using Origin 2018b. Student's *t*-test was performed to measure the significance between
745 the groups. P values < 0.05 were considered statistically significant. Statistical significance for Figure 4D
746 and S3C was determined using the Holm-Sidak method with alpha = 0.05. Each row was analyzed
747 individually, without assuming a consistent SD (number of *t* tests = 10 and 2 for Figure 4D, and S3C,
748 respectively). Statistical significance for differential gene expression in Figures 4F and Figure S4G was
749 determined using the Cell Ranger 2.1.1 algorithm. Sample pairs with each genotype were analyzed and
750 clustered with individual Cell Ranger runs for each pair and analyzed using the Loupe Cell Browser (v.2.0.0).

Differential expression was calculated using a negative binomial exact test, and p values were adjusted using the Benjamini-Hochberg correction for multiple tests. P <0.01 was used as the threshold for assigning significant versus non-significant changes in gene expression. Volcano plots were generated in RStudio (v 1.1.456) using the ggplot2 package. For Figures 3K, L, M, and S3B, discovery was determined using the two-stage linear step-up procedure of Benjamini, Krieger, and Yekutieli with Q = 1%. Each row was analyzed individually, without assuming a consistent SD (number of *t* tests = 3).

Data and Software availability

Upon acceptance, scRNA-seq data will be posted to an accession database. Raw targeted sequencing files for DNA and RNA sequencing data will be deposited to the NCBI Trace and Short-Read Archive. Raw patch clamp data are available upon request. Other experimental data are provided in Supplemental files and all source data are available upon request.

773 **Supporting Information:**

774 **Figure S1**

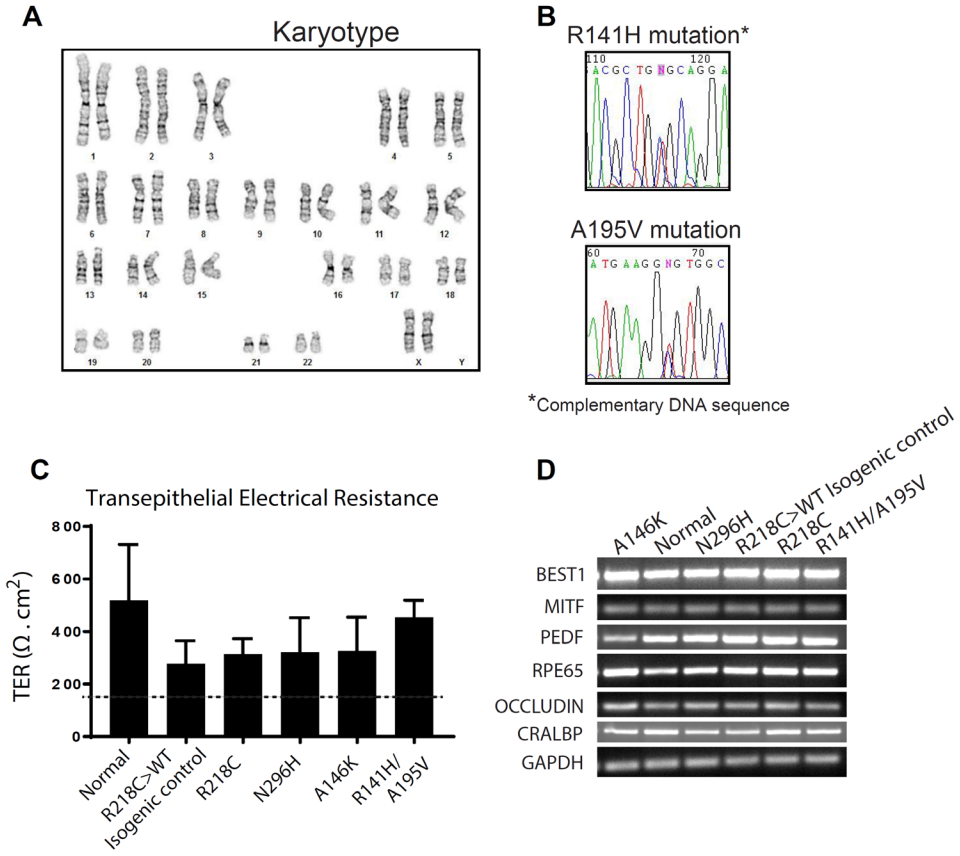

775

Figure S1 | Characterization of iPSC-RPE. (A) Karyotype analysis for ARB iPSCs. **(B)** DNA sequencing confirming R141H and A195V encoding mutations in ARB iPSCs. **(C)** Net transepithelial electrical resistance (TER) ($\Omega \cdot cm^2$) for iPSC-RPE from all six lines. The dashed line demarcates the minimum expected TER (150 $\Omega \cdot cm^2$). Replicates: n=12 for each line (4 transwells from 3 replicates each), error bars represent mean ± SD. **(D)** Gene expression analysis (RT-PCR) of selected RPE-specific markers in all six lines. **(E-J)** Chloride current traces, measured in the presence (*black*) or absence (*gray*) of calcium over a voltage ramp (-100 to +100 mV), that were used to generate CaCC current density plots in Figure 1E. 4.5 μM calcium was used for +calcium conditions. The number (n) of individual cells patch clamped in the presence or absence of calcium in order to calculate CaCC current densities is shown in the top left corner of each graph. Data were obtained from at least two replicates.

Figure S2

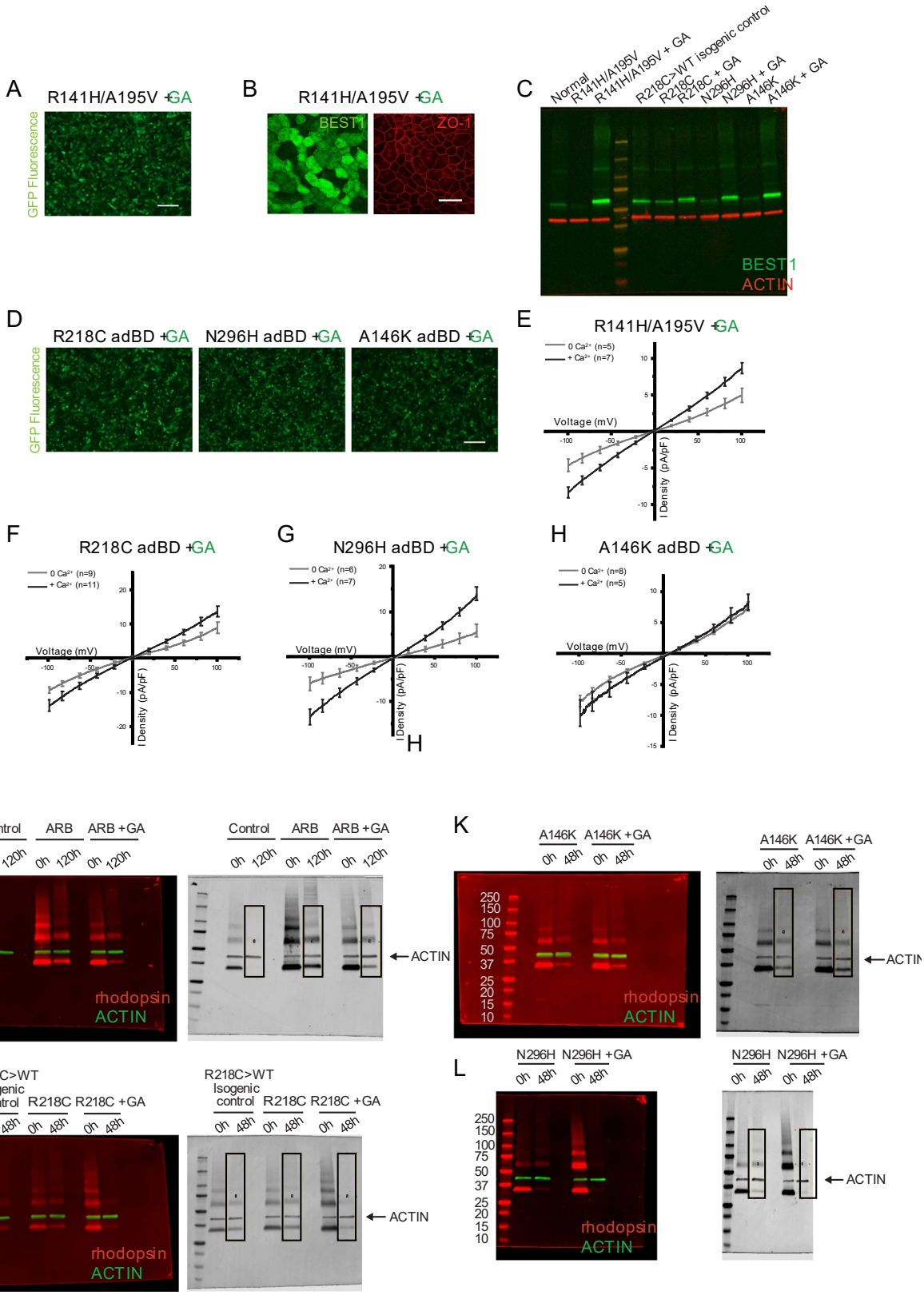

788 **Figure S2 | Gene augmentation (GA) restores CaCC function in ARB iPSC-RPE and R218C and**
789 **N296H adBD iPSC-RPE, but not in A146K adBD iPSC-RPE. (A)** GFP fluorescence in R141H/A195V
790 ARB iPSC-RPE transduced with lentivirus expressing BEST1. Scale bar = 100 µm. **(B)** ICC analysis of
791 BEST1 and ZO-1 expression in R141H/A195V iPSC-RPE transduced with lentivirus expressing BEST1.
792 Increased BEST1 expression is observed in R141H/A195V iPSC-RPE cells following gene augmentation.
793 Scale bar = 50 µm (applies to both images). **(C)** Representative western blot showing levels of BEST1 in
794 iPSC-RPE. Protein samples from the rhodopsin degradation assays were used to assess BEST1 levels. **(D)**
795 GFP fluorescence in adBD iPSC-RPE transduced with lentivirus expressing hBEST1. Scale bar = 100 µm
796 (applies to all three images). **(E)** Chloride current traces of R141H/A195V iPSC-RPE after gene
797 augmentation measured in the presence (*black*) or absence (*gray*) of calcium. **(F-H)** Chloride current
798 traces for adBD iPSC-RPE after gene augmentation, measured in the presence (*black*) or absence (*gray*)
799 of calcium over a voltage ramp (-100 to +100 mV), that were used to obtain CaCC current density. 4.5
800 µM calcium was used for +calcium conditions. Cells with green fluorescence were used for all patch
801 clamp measurements after gene augmentation. The number (n) of individual cells patch clamped in the
802 presence or absence of calcium (in order to calculate CaCC current densities) is shown in the top left
803 corner of each graph. Data were obtained from at least two replicates. **(I-L)** *left*, Western blots used for
804 the rhodopsin degradation assay, *right*, and corresponding grayscale images of western blots used to
805 quantify levels of rhodopsin shown in Figures 2 and 3 (boxes represent areas used for quantification). For
806 each lane, the boxed area was selected to include bands corresponding to fully denatured rhodopsin and
807 its aggregated forms.
808

Figure S3

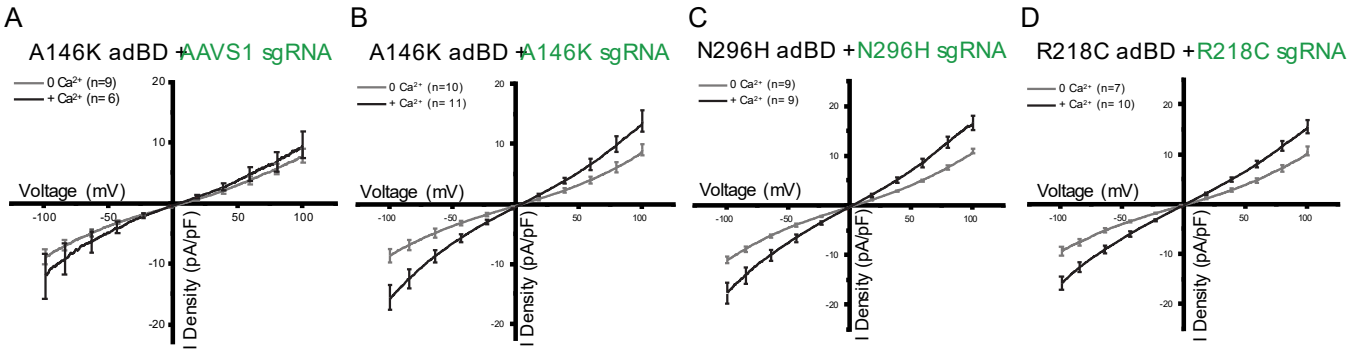

Figure S3 | Gene editing (GE) restores CaCC activity in iPSC-RPE from all tested adBD lines. (A-D) Chloride current traces, measured in the presence (*black*) or absence (*gray*) of calcium over a voltage ramp (-100 to +100 mV), that were used to calculate CaCC current density plots after gene editing of adBD iPSC-RPE. iPSC-RPE was edited using lentiviral genome editors encoding sgRNA targeting **(A)** *AAVS1* site in A146K adBD iPSC-RPE, **(B)** A146K mutation in A146K adBD iPSC-RPE, **(C)** N296H mutation in N296H adBD iPSC-RPE, or **(D)** R218C mutation in R218C adBD iPSC-RPE. Cells with GFP fluorescence were used for whole cell patch clamp measurements and 4.5 µM calcium was used for +calcium conditions. The number (n) of individual cells patch clamped with or without calcium is shown at the top left corner of each graph. Data were obtained from two replicates.

Figure S4

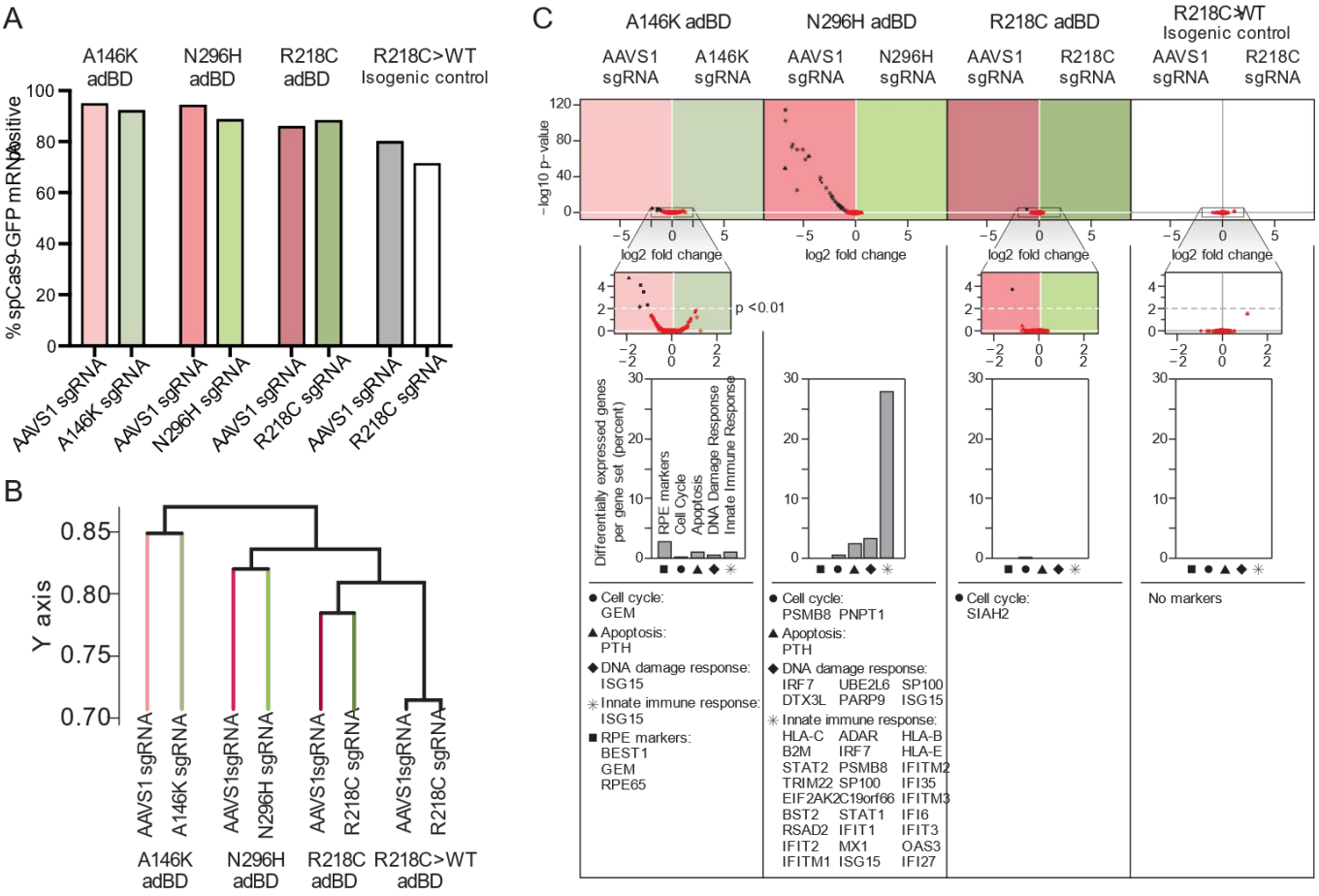

Figure S4 | Single cell transcriptome analysis in gene-edited adBD iPSC-RPE. (A) Percent of analyzed cells per sample for which *spCas9-T2A-GFP* transcripts were captured using scRNA-seq. **(B)** Dendrogram tree depicting relative similarity between samples. Non-negative matrix factorization comparison across samples indicates that greater transcriptional variability exists between iPSC-RPE lines than in the same iPSC-RPE line treated with lentiviral genome editors (*AAVS1* lentiviral genome editor versus *BEST1* mutant allele-targeted lentiviral genome editor). The dendrogram shows the similarity of the transcriptomes from each sample, derived from the average Jaccard coefficient between gene clusters from one sample and those from another sample. The y-axis denotes 1-average Jaccard coefficient and

838 indicates the distance between different samples (tree tips) as well as between groups of samples (internal
839 nodes). **(C)** Differential gene expression in 5 curated gene sets associated with cell cycle regulation
840 (*circles*), apoptosis (*triangles*), DNA damage response (*diamonds*), innate immune response (*asterisks*),
841 or RPE-identity (*squares*) in control (*AAVS1*) lentiviral genome editor versus mutant allele-targeted
842 lentiviral genome editor treated samples. For one sample pair (N296H iPSC-RPE), genes associated with
843 a potential adverse treatment effect were upregulated in control lentiviral genome editor-treated sample
844 compared to the mutant allele-targeted lentiviral genome editor sgRNA-treated sample.
845
846 **SI Tables (**attached below**):**
847 Table S1: RPE-specific RT-PCR primers used.
848 Table S2. List of GE vectors used.
849 Table S3. List of primers for lentiviral plasmid generation.
850 Table S4. List of sgRNAs.
851 Table S5. Primers for deep sequencing of DNA and cDNA.
852
853 **SI data files (**available for download**):**
854 SI Data File A. Frameshift analysis of iPSC-RPE+GE.
855 SI Data File B. Curated gene sets used to assess differences in gene expression between control (*AAVS1*)
856 and mutant *BEST1* allele-targeted sgRNA.
857 SI Data File C. Ranked off-target sites for sgRNAs used in this study.
858 SI Data File D. Analysis of additional adBD mutations for amenability to allele-specific editing or
859 scarless base editing.

860 **SI Tables:**

861 **Table S1: RPE-specific RT-PCR primers used.**

862

Gene	**Forward Primer**	**Reverse Primer**
BEST1	ATTTATAGGCTGGCCCTCACGGAA	TGTTCTGCCGGAGTCATAAAGCCT
MITF	TTCACGAGCGTCCTGTATGCAGAT	TTGCAAAGCAGGATCCATCAAGCC
PEDF	AATCCATCATTCACCGGGCTCTCT	TGCACCCAGTTGTTGATCTCTTGC
RPE65	GCCCTCCTGCACAAGTTTGACTTT	AGTTGGTCTCTGTGCAAGCGTAGT
OCCLUDIN	TCATTGCCGCGTTGGTGATCTTTG	ATGATGCCCAGGATAGCACTCACT
CRALBP	TTCCGCATGGTACCTGAAGAGGAA	ACTGCAGCCGGAAATTCACATAGC
GAPDH	CAACGGATTTGGTCGTATTGG	GCAACAATATCCACTTTACCACAGTTAA

863
864

865 **Table S2. List of gene editing vectors used.**
866

GE Vector Name	sgRNA Name	Vector Backbone	Backbone Source
VMD2.*AAVS1*	*AAVS1*	*hVMD2-spCas9-T2A-GFP*	Alfred Lewin (University of Florida)
VMD2.R218C	R218C	*hVMD2-spCas9-T2A-GFP*	Alfred Lewin (University of Florida)
VMD2.N296H	N296H	*hVMD2-spCas9-T2A-GFP*	Alfred Lewin (University of Florida)
VMD2.A146K	A146K	*hVMD2-spCas9-T2A-GFP*	Alfred Lewin (University of Florida)

867

868 **Table S3. List of primers for lentiviral plasmid generation.**
869

Primer Name	Primer sequence
LCv2-GFP.Gib.F	GATTACAAAGACGATGACGATAAGGGATCCGGTGAGGGCAGAGGAAGTC
LCv2-GFP.Gib.	ACAGTCGAGGCTGATCAGCGGGTTTAAACCTACTACTGCTAGAGATTTTCCACAC
LCv2-GFP.seq.L	ACCGGCCTGTACGAGACACG
LCv2-GFP.seq.R	GAAAGGACAGTGGGAGTGGCACC
VMD2.LCv2.GFP.Gib.F	GTGGCACCGAGTCGGTGCTTTTTTGAATTCCAATTCTGTCATTTTACTAGGGTGATGAAATTC
VMD2.LCv2.GFP.Gib.R	TGTACTTCTTGTCCATGGTGGCAGCGCTCTATCGGCCGCGGGTACA
VMD2.LCv2.GFP.seq.L	GAATGAATACCGGGCTGCAGTCAAC
VMD2.LCv2.GFP.seq.R	GTCGGTGATCACGGCCCAG

870
871

872 **Table S4. List of sgRNAs.**

873

874 Off-target (47) and on-target (48) scores are also presented. Scores range from 0-100 with higher scores
875 being better for both scoring systems. Highest ranked off-target cut sites for each sgRNA are available in
876 **SI Data File C**.

877

sgRNA Name	Sequence 5' - 3'	PAM	Chr	Position	Strand	Off-Target Score	On-Target Score
A146K	CTTTGGTGCTGACGCTGCGC	AGG	11	61955893	-1	81.2	51.6
R218C	GTGTCCACACTGAGTACACA	AGG	11	61957403	-1	56.3	67.2
N296H	CATCATCCTCTCCAAAGGGG	TGG	11	61959521	-1	54.0	64.6
AAVS1	GGGGCCACTAGGGACAGGAT	TGG	19	55115755	+1	55.8	54.5

878

879 **Table S5. Primers for deep sequencing of DNA and cDNA.**
880

Primer Name	Primer sequence
MT.C.OT.5v2.HTS.F	GTTGGTTCCTGAAGATGGGCAG
MT.C.OT.5v2.HTS.R	CTGTCAAGGCCAAGTTCTGCTG
MT.C.OT.2.HTS.F	GCTAAATTCTGCTATAAAAGGAAGG
MT.C.OT.2.HTS.R	GCATTGCTTTAGAAAACTCAGAAGT
MT.C.OT.3.HTS.F	AGTGAGACCAAGTTCTGACAGCA
MT.C.OT.3.HTS.R	GGCCTCTTCATACATACACATGCAC
MT.C.OT.4.HTS.F	CCTCCACATCTGCAGAAAAGTGT
MT.C.OT.4.HTS.R	GGCAGGGTTTGGTCTCCTACTT
MT.C.OT.5.HTS.F	GGATGGCTCTGGGTGGGTTT
MT.C.OT.5.HTS.R	CTTCCAACTCTTCCTCCCACCC
MT.C.OT.6.HTS.F	TGAGGTTCAGAATAGCTCAGCA
MT.C.OT.6.HTS.R	TGTTTCTGTGAAGCAAATCAAAGCT
MT.C.OT.7.HTS.F	TGTTTCTGTGAAGCAAATCAAAGCT
MT.C.OT.7.HTS.R	TGAGGTTCAGAATAGCTCAGCA
MT.C.OT.8.HTS.F	AAAGCATGGCGGGAGTGCTAA
MT.C.OT.8.HTS.R	TGACTAAATCCCTGGCATCGCT
MT.C.OT.9.HTS.F	GCCAGTAATTTTCCAAGGCTTCT
MT.C.OT.9.HTS.R	TTCCTACTAGAACCTCCTTGAG
MT.C.OT.10.HTS.F	GTGACCTGACTTTGCTGAAAGGT
MT.C.OT.10.HTS.R	ACCTGAATTATCTCAAGCTCACT
AAVS1T2.HTS.F	ATGTGGCTCTGGTTCTGGGTAC
AAVS1T2.HTS.R	GAGACTAGGAAGGAGGAGGCCT
R218C.HTSv2.F	GTGTTCAGAACCCCATCCCC
R218C.HTSv2.R	AGCCTAGTCCTCACCTGTGT
BEST.cDNA.HTSv2.F	GGTCGAATCCGGGACCCTATC
BEST.cDNA.HTSv2.R	GCCACAGTCACCACCTGTGTAT
AAVS1T2.HTS.F	ATGTGGCTCTGGTTCTGGGTAC
AAVS1T2.HTS.R	GAGACTAGGAAGGAGGAGGCCT

881
882

References

1. J. A. Doudna, E. Charpentier, The new frontier of genome engineering with CRISPR-Cas9. *Science* **346**, 1077-+ (2014).
2. B. L. Lam *et al.*, Choroideremia Gene Therapy Phase 2 Clinical Trial: 24-Month Results. *Am J Ophthalmol* **197**, 65-73 (2019).
3. C. Cukras *et al.*, Retinal AAV8-RS1 Gene Therapy for X-Linked Retinoschisis: Initial Findings from a Phase I/IIa Trial by Intravitreal Delivery. *Mol Ther* **26**, 2282-2294 (2018).
4. S. Russell *et al.*, Efficacy and safety of voretigene neparvovec (AAV2-hRPE65v2) in patients with RPE65-mediated inherited retinal dystrophy: a randomised, controlled, open-label, phase 3 trial. *Lancet* **390**, 849-860 (2017).
5. H. Ledford, FDA advisers back gene therapy for rare form of blindness. *Nature* **550**, 314 (2017).
6. B. Bakondi *et al.*, In Vivo CRISPR/Cas9 Gene Editing Corrects Retinal Dystrophy in the S334ter-3 Rat Model of Autosomal Dominant Retinitis Pigmentosa. *Mol Ther* **24**, 556-563 (2016).
7. Y. T. Tsai *et al.*, Clustered Regularly Interspaced Short Palindromic Repeats-Based Genome Surgery for the Treatment of Autosomal Dominant Retinitis Pigmentosa. *Ophthalmology* **125**, 1421-1430 (2018).
8. P. Li, Kleinstiver, B.P., Leon, M.Y., Prew, M.S., Navarro-Gomez, D., Greenwald, S.H., Pierce, E.A., Joung, J.K., Liu, Q., Allele-Specific CRISPR-Cas9 Genome Editing of the Single-Base P23H Mutation for Rhodopsin-Associated Dominant Retinitis Pigmentosa. *The CRISPR Journal* **1**, 55-64 (2018).
9. V. Pattanayak *et al.*, High-throughput profiling of off-target DNA cleavage reveals RNA-programmed Cas9 nuclease specificity. *Nat Biotechnol* **31**, 839-843 (2013).
10. D. G. Courtney *et al.*, CRISPR/Cas9 DNA cleavage at SNP-derived PAM enables both in vitro and in vivo KRT12 mutation-specific targeting. *Gene Ther* **23**, 108-112 (2016).
11. M. K. Cromer *et al.*, Global Transcriptional Response to CRISPR/Cas9-AAV6-Based Genome Editing in CD34(+) Hematopoietic Stem and Progenitor Cells. *Mol Ther* **26**, 2431-2442 (2018).
12. S. Lessard *et al.*, Human genetic variation alters CRISPR-Cas9 on- and off-targeting specificity at therapeutically implicated loci. *Proc Natl Acad Sci U S A* **114**, E11257-E11266 (2017).
13. M. L. Maeder *et al.*, Development of a gene-editing approach to restore vision loss in Leber congenital amaurosis type 10. *Nat Med* **25**, 229-233 (2019).
14. K. E. Guziewicz *et al.*, Bestrophinopathy: An RPE-photoreceptor interface disease. *Prog Retin Eye Res* **58**, 70-88 (2017).
15. A. A. Johnson *et al.*, Bestrophin 1 and retinal disease. *Prog Retin Eye Res* **58**, 45-69 (2017).
16. V. K. Dickson, L. Pedi, S. B. Long, Structure and insights into the function of a Ca2+-activated Cl- channel. *Nature* **516**, 213-218 (2014).
17. R. Singh *et al.*, iPS cell modeling of Best disease: insights into the pathophysiology of an inherited macular degeneration. *Hum Mol Genet* **22**, 593-607 (2013).
18. R. Singh *et al.*, Pharmacological Modulation of Photoreceptor Outer Segment Degradation in a Human iPS Cell Model of Inherited Macular Degeneration. *Mol Ther* **23**, 1700-1711 (2015).
19. B. Steyer *et al.*, Scarless Genome Editing of Human Pluripotent Stem Cells via Transient Puromycin Selection. *Stem Cell Reports* **10**, 642-654 (2018).
20. A. Milenkovic, V. M. Milenkovic, C. H. Wetzel, B. H. F. Weber, BEST1 protein stability and degradation pathways differ between autosomal dominant Best disease and autosomal recessive bestrophinopathy accounting for the distinct retinal phenotypes. *Hum Mol Genet* **27**, 1630-1641 (2018).
21. A. D. Marmorstein *et al.*, Mutant Best1 Expression and Impaired Phagocytosis in an iPSC Model of Autosomal Recessive Bestrophinopathy. *Sci Rep* **8**, 4487 (2018).
22. K. E. Guziewicz *et al.*, BEST1 gene therapy corrects a diffuse retina-wide microdetachment modulated by light exposure. *P Natl Acad Sci USA* **115**, E2839-E2848 (2018).

23. Y. Li *et al.*, Patient-specific mutations impair BESTROPHIN1's essential role in mediating Ca(2+)-dependent Cl(-) currents in human RPE. *Elife* **6** (2017).
24. N. Waugh *et al.*, Treatments for dry age-related macular degeneration and Stargardt disease: a systematic review. *Health Technol Assess* **22**, 1-168 (2018).
25. P. K. Shahi *et al.*, Gene Augmentation and Readthrough Rescue Channelopathy in an iPSC-RPE Model of Congenital Blindness. *Am J Hum Genet* **104**, 310-318 (2019).
26. D. B. Cox, R. J. Platt, F. Zhang, Therapeutic genome editing: prospects and challenges. *Nat Med* **21**, 121-131 (2015).
27. M. W. Popp, L. E. Maquat, Leveraging Rules of Nonsense-Mediated mRNA Decay for Genome Engineering and Personalized Medicine. *Cell* **165**, 1319-1322 (2016).
28. R. G. H. Lindeboom, M. Vermeulen, B. Lehner, F. Supek, The impact of nonsense-mediated mRNA decay on genetic disease, gene editing and cancer immunotherapy. *Nat Genet* **51**, 1645-1651 (2019).
29. M. Sadelain, E. P. Papapetrou, F. D. Bushman, Safe harbours for the integration of new DNA in the human genome. *Nat Rev Cancer* **12**, 51-58 (2011).
30. M. W. Shen *et al.*, Predictable and precise template-free CRISPR editing of pathogenic variants. *Nature* **563**, 646-651 (2018).
31. C. J. Boon *et al.*, The spectrum of ocular phenotypes caused by mutations in the BEST1 gene. *Prog Retin Eye Res* **28**, 187-205 (2009).
32. C. Ji *et al.*, Investigation and Restoration of BEST1 Activity in Patient-derived RPEs with Dominant Mutations. *Sci Rep* **9**, 19026 (2019).
33. A. A. Johnson *et al.*, Disease-causing mutations associated with four bestrophinopathies exhibit disparate effects on the localization, but not the oligomerization, of Bestrophin-1. *Exp Eye Res* **121**, 74-85 (2014).
34. V. Vasireddy *et al.*, AAV-mediated gene therapy for choroideremia: preclinical studies in personalized models. *PLoS One* **8**, e61396 (2013).
35. G. Vaisey, A. N. Miller, S. B. Long, Distinct regions that control ion selectivity and calcium-dependent activation in the bestrophin ion channel. *Proc Natl Acad Sci U S A* **113**, E7399-E7408 (2016).
36. A. V. Cideciyan *et al.*, Mutation-independent rhodopsin gene therapy by knockdown and replacement with a single AAV vector. *Proc Natl Acad Sci U S A* **115**, E8547-E8556 (2018).
37. P. Mali *et al.*, RNA-guided human genome engineering via Cas9. *Science* **339**, 823-826 (2013).
38. B. Wienert, J. Shin, E. Zelin, K. Pestal, J. E. Corn, In vitro-transcribed guide RNAs trigger an innate immune response via the RIG-I pathway. *PLoS Biol* **16**, e2005840 (2018).
39. A. L. George, Jr., Inherited Channelopathies Associated with Epilepsy. *Epilepsy Curr* **4**, 65-70 (2004).
40. C. P. Schaaf, Nicotinic acetylcholine receptors in human genetic disease. *Genet Med* **16**, 649-656 (2014).
41. C. Villa, R. Combi, Potassium Channels and Human Epileptic Phenotypes: An Updated Overview. *Front Cell Neurosci* **10**, 81 (2016).
42. R. Singh *et al.*, Functional analysis of serially expanded human iPS cell-derived RPE cultures. *Invest Ophthalmol Vis Sci* **54**, 6767-6778 (2013).
43. A. Kuruma, H. C. Hartzell, Bimodal control of a Ca(2+)-activated Cl(-) channel by different Ca(2+) signals. *J Gen Physiol* **115**, 59-80 (2000).
44. L. Pinello *et al.*, Analyzing CRISPR genome-editing experiments with CRISPResso. *Nat Biotechnol* **34**, 695-697 (2016).
45. N. V. Strunnikova *et al.*, Transcriptome analysis and molecular signature of human retinal pigment epithelium. *Hum Mol Genet* **19**, 2468-2486 (2010).
46. D. D. Lee, H. S. Seung, Algorithms for Non-negative Matrix Factorization. *Advances in Neural Information Processing Systems* **13**, 556-562 (2000).
47. J. G. Doench *et al.*, Optimized sgRNA design to maximize activity and minimize off-target effects of CRISPR-Cas9. *Nat Biotechnol* **34**, 184-191 (2016).

48. P. D. Hsu *et al.*, DNA targeting specificity of RNA-guided Cas9 nucleases. *Nat Biotechnol* **31**, 827-832 (2013).